NASA CONTRACTOR REPORT

NASA CR-1354

EXPERIMENTAL EVALUATION OF A SUBSONIC EXPANSION TUBE

by Philip C. Malte and Kenneth R. Sivier

Prepared by
UNIVERSITY OF MICHIGAN
Ann Arbor, Mich.
for Lewis Research Center

NATIONAL AERONAUTICS AND SPACE ADMINISTRATION • WASHINGTON, D. C. • JUNE 1969

NASA CR-1354

EXPERIMENTAL EVALUATION OF A SUBSONIC EXPANSION TUBE

By Philip C. Malte and Kenneth R. Sivier

Prepared under Grant No. NGR 23-005-003 by
UNIVERSITY OF MICHIGAN
Ann Arbor, Mich.

for Lewis Research Center

NATIONAL AERONAUTICS AND SPACE ADMINISTRATION

For sale by the Clearinghouse for Federal Scientific and Technical Information
Springfield, Virginia 22151 – CFSTI price $3.00

ABSTRACT

An experimental study of a subsonic expansion tube was carried out to determine its utility as a test facility for studying the drag of small spherical particles at subsonic Mach numbers and Reynolds numbers below 1000. Of particular interest were the length of "steady" flow achieved, the steadiness of this flow, the tube geometry needed to optimize the flow quality, and the growth of the unsteady boundary layer on the tube walls. It was found that a 15 ft long tube was capable of providing useful flows for at least 15 msec for Mach numbers up to about 0.7.

FOREWORD

This research was part of an investigation, entitled "The Study of the Dynamics of Inert and Reacting Particles in the Exhaust of Solid Rocket Nozzles," that was supported by NASA Grant NsG 86-60. The research was under the technical cognizance of H. Bankaitis, NASA Lewis Research Center, and was conducted at the Gas Dynamics Laboratories, Department of Aerospace Engineering, The University of Michigan, under the direction of Professor J.A. Nicholls. The authors wish to thank Professor A. F. Messiter for his helpful discussions and suggestions and to acknowledge the contributions of Stephen C. Schmidt who carried out much of the design, assembly, and preliminary testing of the expansion tube.

TABLE OF CONTENTS

LIST OF FIGURES

NOMENCLATURE

a	speed of sound
A_p	cross-sectional area of pipe
A_o	cross-sectional area of orifice opening
C_D	particle drag coefficient
d	particle diameter
d_p	pipe diameter
$g(s)$	percentage change in s/msec behind expansion wave
ℓ	length of tube
ℓ_o	distance between tube exit and observation point
M	Mach number
P	pressure
ΔP_s	drop in static pressure across expansion wave
ΔP_t	drop in total pressure across expansion wave
$\overline{P}(s)$	probable error in s
q	dynamic pressure
r	radial distance from pipe centerline
r_p	pipe radius
R	gas constant
Re	Reynolds number based on particle or pipe diameter
Re_X	Reynolds number based on X
s	generalized flow or fluid variable
Δs	change in s over time interval Δt
t	time
Δt	time interval between measurements behind expansion wave
t_R	test time for $\ell_o = 0$
t_L	test time lost for $\ell_o \neq 0$
t_T	test time for $\ell_o \neq 0$

T	temperature
u	gas velocity
v_p	particle velocity
V_{tank}	volume of dump tank
x	longitudinal distance along tube centerline measured positively from open end of tube
x_p	particle displacement
X	distance slug of gas has travelled when it reaches observation point
α	particle acceleration
δ	boundary layer thickness
γ	ratio of specific heats
ϕ	axial velocity ratio (v_p/u)
ρ	gas density
ρ_P	particle density
μ	viscosity

Subscripts

1	initial conditions in tank
3	flow variable (except stagnation quantities) in region behind expansion wave
3s	experimental Mach number based on P_4/P_3
3t	stagnation quantities behind expansion wave and experimental Mach number based on P_{3t}/P_3
4	initial conditions in tube
7	experimental measurement at 7 msec after arrival of expansion wave head at observation point
22	experimental measurement at 22 msec after arrival of expansion wave head at observation point
ave	average value of s over time interval Δt
c	rocket chamber conditions

e	tube exit conditions
f	time (after passage of head of expansion wave at observation point) for second experimental measurement, usually 22 msec
g	gas conditions
i	time (after passage of head of expansion wave at observation point) for first experimental measurement, usually 7 msec

Superscripts

*	average value of flow variable in central core of gas (outside of boundary layer) at one measurement time

1. INTRODUCTION

Recently, at The University of Michigan, there has been interest in obtaining particle drag coefficients pertinent to two phase flow in solid propellant rocket nozzles. In Fig. 1 (which has been reproduced from Ref. 1) it is seen that the subsonic slip flow regime is of substantial importance in such a study. A recent investigation by Selberg[2] employed a shock tube to accelerate small, nonburning particles in continuum flow at incompressible Mach numbers; the particle sizes ranging from 150 to 450 μ. However, these experiments were limited by the short period of useful flow that is inherent in shock tube experiments. For the 16 ft, constant area, single diaphragm shock tube used in Selberg's experiments, the test time was no more than 5 msec for incompressible continuum flow. The available testing time in this shock tube decreased rapidly for Mach numbers above about 0.5.

Theoretical analyses indicated that sufficient test time for the acquisition of subsonic compressible slip flow drag coefficients of small burning and nonburning particles could be obtained in a simple expansion tube. In this device, a centered expansion wave propagates into the tube after a diaphragm is burst at the open end of the tube. A wave diagram of the subsonic expansion tube is shown in Fig. 2. Aerodynamic testing can be carried out in the quasi-steady flow occurring between the passage of the

centered expansion wave and reflected head of the wave. It should be noted that this device is limited to subsonic Mach numbers, since as sonic flow is approached, the centered expansion wave tends to fill the tube and the period of quasi-steady flow rapidly shrinks to zero.

It was the object of this investigation to evaluate experimentally the performance of a subsonic expansion tube as a device suitable for studying the drag of particles in subsonic compressible slip flow. In particular, it was desired to obtain information about the operating characteristics of the expansion tube with special emphasis on flow steadiness, length of 'steady' flow, and the tube geometry necessary to optimize the 'steady' flow. These studies were carried out at test conditions related to the particle drag problem; i.e., particle Reynolds numbers (based on particle diameter) below 1000. Assuming that particle drag studies would be conducted using 1/64 in. diameter spheres, the maximum Reynolds number (based on a tube diameter of 3.1 in.) of the expansion tube studies was taken as 1.98×10^5; measurements were made at this value of Re and at 1/10 this value, 1.98×10^4. These operating conditions required tube pressures below atmospheric and thus a dump tank was required at the end of the tube.

In Section 2 below, a theoretical analysis of the expansion tube and its operation is presented. Section 3 presents a discussion of the tube and instrumentation used in this study and a discussion of the experimental procedure

and an error analysis is given in Section 4. Finally, a discussion of the results of this study is found in Section 5.

2. THEORETICAL ANALYSIS

2.1 MACH NUMBER—REYNOLDS NUMBER PERFORMANCE

In using a shock tube (or expansion tube) to make particle drag measurements, the particles are dropped into the tube just ahead of the incident shock (or expansion) wave. The particles are accelerated by the quasi-steady flow behind the wave and their "free" trajectory is recorded optically as a function of time; e.g., see Ref. 2. If the velocity, density, and temperature of the gas behind the wave is known together with the instantaneous values of particle velocity and acceleration, it is possible to determine the instantaneous value of the particle's drag coefficient.

The gasdynamic state of the gas behind the incident wave in the expansion tube can be obtained from the "jump" relations for the starting expansion wave and the initial conditions upstream and downstream of the tube's diaphragm.

The ideal theory for isentropic, time dependent wave systems, Ref. 3, yields the following expressions which describe the flow behind the centered expansion wave in terms of the stationary gas properties ahead of the wave:

$$u_3 = \frac{2a_4}{\gamma - 1}\left[1 - \left(\frac{P_3}{P_4}\right)^{(\gamma-1)/2\gamma}\right] \qquad (1)$$

$$a_3 = a_4 \left(\frac{P_3}{P_4}\right)^{(\gamma-1)/2\gamma} \tag{2}$$

$$M_3 = \frac{2}{\gamma - 1}\left[\left(\frac{P_4}{P_3}\right)^{(\gamma-1)/2\gamma} - 1\right] \tag{3}$$

$$\rho_3 = \frac{P_4}{RT_4}\left(\frac{P_3}{P_4}\right)^{1/\gamma} \tag{4}$$

$$T_3 = T_4 \left(\frac{P_3}{P_4}\right)^{(\gamma-1)/\gamma} \tag{5}$$

For a particle accelerating in the flow behind an expansion wave, the Reynolds number and Mach number of the particle, relative to the test gas, are:

$$Re = \frac{\rho_3 (u_3 - v_p)\, d}{\mu_3} \tag{6}$$

$$M = \frac{u_3 - v_p}{a_3} \tag{7}$$

The particle motion is assumed to be in the direction of the flow. For short test times and low particle accelerations, the particle velocity remains small; i.e.,

$$v_p \ll u_3$$

Thus

$$Re \cong \frac{\rho_3 u_3 d}{\mu_3} \tag{8}$$

$$M \cong M_3 = \frac{u_3}{a_3} \tag{9}$$

If Eq. (1), (3), and (4) are used to replace ρ_3 and u_3 in Eq. (8), Re can be expressed as

$$Re = \frac{P_4 a_4 d M_3}{RT_4 \mu_3(M_3)} \left[\frac{1}{1 + \frac{\gamma - 1}{2} M_3}\right]^{(\gamma+1)/\gamma-1} \tag{10}$$

where μ_3 is a function of T_3 which in turn is related to M_3; μ_3 can be found as a function of M_3 by using the tables of Ref. 4, along with Eq. (5). For the temperatures encountered in the expansion tube operating with air initially at room temperature ($530^{\circ}R$), the relation for the viscosity in lbm/ft-sec is

$$\mu_3 = (1.90 \times 10^{-6}) + (.0196 \times 10^{-6})\, T_4 \left(\frac{5}{5 + M_3}\right)^2 \tag{11}$$

These relationships have been used to obtain M_3 as a function of $P_4 d$ for constant values of Re; the results are presented in Fig. 3 for several values of Re of interest to the particle drag problem. In this plot $\gamma = 1.4$, R = gas constant for ideal air, and $T_4 = 530^{\circ}R$. As an example of the use of

Fig. 3, if M_3 versus P_4 for 1/64 in. diameter particles is desired, the abscissa should be multiplied by 64.

Applying Newton's Second Law to an accelerating particle

$$\rho_P \frac{4}{3} \pi \left(\frac{d}{2}\right)^3 \alpha = \frac{1}{2} \rho_3 (u_3 - v_p)^2 C_D \pi \left(\frac{d}{2}\right)^2 \tag{12}$$

Again noting that $v_p \ll u_3$, the particle acceleration can be expressed as

$$\alpha \cong \frac{3\rho_3 u_3^2 C_D}{4\rho_P d} \tag{13}$$

If Eq. (1), (3), (4), and (10) are substituted into Eq. (13), the particle acceleration becomes

$$\alpha = \frac{3\gamma RT_4 \ \mu_3(M_3) \ M_3 \ Re}{4\rho_P d^2 a_4 \left[1 + \frac{\gamma - 1}{2} M_3\right]} C_D(Re) \tag{14}$$

where it is assumed that the drag coefficient is a function of Reynolds number only and is equal to the steady state experimental value found in Ref. 5. For particle Mach numbers below 0.3, the effect of compressibility is negligible and C_D is a function of Re only; for higher subsonic Mach numbers the drag coefficient does depend upon Mach number. However, since the expansion tube only can be operated satisfactorily for $M_3 \leq 0.8$, and since only a first order solution is of interest here, the effect of Mach number on C_D is neglected. In Fig. 4, the acceleration

parameter $\alpha \rho_p d^2$ is plotted versus M_3 for the range of Reynolds numbers of interest. Again, if M_3 versus α for 1/64 in. diameter, sapphire particles is desired, the abscissa of Fig. 4 should be multiplied by 531.26.

For constant flow conditions and short test times the drag coefficient is essentially constant since Re ≅ constant. Therefore, the acceleration of the particle is approximately constant and for zero initial particle velocity and a zero thickness expansion wave, the particle displacement in t sec is

$$x_p = \frac{\alpha t^2}{2} \tag{15}$$

2.2 TEST TIME

The test time at a given observation point is defined as the time between the passage of the tail of the incident expansion wave and the passage of the head of the reflected expansion wave, see Fig. 2. The equation that describes the path of the reflected expansion wave head as it passes through the remainder of the incident wave is found in Ref. 6; for the coordinate system shown in Fig. 2 it is

$$x = -\frac{2}{\gamma - 1} a_4 t + \frac{\gamma + 1}{\gamma - 1} \ell \left(\frac{a_4 t}{\ell} \right)^{(3-\gamma)/\gamma+1} \tag{16}$$

The path of the tail of the expansion wave before reflection is

$$x/t = a_3 - u_3 \tag{17}$$

The intersection point (x_i, t_i) is defined as the point where the tail and reflected head meet; using Eq. (1), (2), (3), (16) and (17) the intersection point is found to be:

$$t_i = \frac{\ell}{a_4}\left(1 + \frac{\gamma - 1}{2} M_3\right)^{(\gamma+1)/2(\gamma-1)} \tag{18}$$

$$x_i = \frac{a_4 (1 - M_3)}{\left(1 + \frac{\gamma - 1}{2} M_3\right)} t_i \tag{19}$$

After intersection the path of the head of the reflected expansion wave is expressed by

$$\frac{x - x_i}{t - t_i} = - (a_3 + u_3) = - \frac{a_4 (1 + M_3)}{\left(1 + \frac{\gamma - 1}{2} M_3\right)} \tag{20}$$

The time for the reflected head to travel from the intersection point to the point of origin of the expansion wave, i.e., point of diaphragm rupture, is

$$t_a = \left(\frac{1 - M_3}{1 + M_3}\right) t_i \tag{21}$$

The test time at the point of diaphragm rupture can therefore be expressed as

$$t_R = t_a + t_i = \frac{2}{1 + M_3} t_i \tag{22}$$

In the actual expansion tube, a small amount of test time is lost by making measurements at a point slightly upstream from the point of

diaphragm rupture; this is necessary to insure a well formed flow at the observation point and to avoid three-dimensional effects in the vicinity of the orifice plate. If ℓ_o is the distance from the tube exit to the observation point, the time lost, t_L, is expressed as

$$t_L = \frac{\ell_o}{(a_3 - u_3)} + \frac{\ell_o}{(a_3 + u_3)} = \frac{2\ell_o}{a_4}\left(\frac{\frac{\gamma - 1}{2} M_3 + 1}{1 - M_3^2}\right) \tag{23}$$

The theoretical test time at position $x = \ell_o$ for an expansion tube of length ℓ is therefore

$$t_T = t_R - t_L \tag{24}$$

Plots of t_R/ℓ and t_L/ℓ_o are found in Fig. 5 for $\gamma = 1.4$ and $a_4 = 1130.0$ ft/sec; for $\ell_o = 9$ in. and $\ell = 15$ ft, t_T is about 20 msec for $M_3 \leq 0.8$.

2.3 EFFECT OF DIAPHRAGM PRESSURE RATIO AND ORIFICE SIZE ON MACH NUMBER

The initial pressure on the low pressure side of the diaphragm is denoted by P_1, i.e., P_1 is the initial tank pressure. It was found experimentally that the pressure behind the expansion wave in the pipe, P_3, is very nearly equal to P_1 if the pipe exit remains unchoked. That is, the unsteady wave system consists primarily of a centered expansion wave moving upstream in the pipe; the compression system formed by the bursting diaphragm weakens quickly as it spreads into the tank and its effect is

therefore negligible. Thus, it is assumed that all the pressure drop occurs across the expansion wave. Setting $P_3 = P_1$ in Eq. (3), the Mach number of the flow in the pipe accelerated by the expansion wave becomes

$$M_3 = \frac{2}{\gamma - 1}\left[\left(\frac{P_4}{P_1}\right)^{(\gamma-1)/2\gamma} - 1\right] \tag{25}$$

If an orifice is placed at the tube exit, M_3 depends upon P_4/P_1 and A_o/A_p for unchoked flow and only on A_o/A_p for choked flow. Denoting conditions at the orifice by e, and conditions in the pipe by the 3, the pertinent equations become:

$$M_3 = \frac{2}{\gamma - 1}\left[\left(\frac{P_4}{P_3}\right)^{(\gamma-1)/2\gamma} - 1\right] \tag{3}$$

$$P_e\left(1 + \frac{\gamma - 1}{2} M_e^2\right)^{\gamma/(\gamma-1)} = P_3\left(1 + \frac{\gamma - 1}{2} M_3^2\right)^{\gamma/(\gamma-1)} \tag{26}$$

$$\frac{A_o}{A_p} = \frac{M_3}{M_e}\left[\frac{1 + \frac{\gamma - 1}{2} M_e^2}{1 + \frac{\gamma - 1}{2} M_3^2}\right]^{(\gamma+1)/2(\gamma-1)} \tag{27}$$

where Eq. (26) and (27) are the usual equations for steady isentropic flow. If the orifice remains unchoked the exit pressure, P_e, is equal to P_1, and Eq. (3) and (26) can be arranged to yield

$$M_3 = \frac{2}{\gamma - 1}\left[\left(\frac{P_4}{P_1}\right)^{(\gamma-1)/2\gamma}\left(\frac{1 + \frac{\gamma - 1}{2} M_3^2}{1 + \frac{\gamma - 1}{2} M_e^2}\right)^{1/2} - 1\right] \tag{28}$$

where M_e is found from Eq. (26). Combining Eq. (27) and (28) the expression relating M_3, P_4/P_1 and A_o/A_p is

$$\frac{A_o}{A_p} = \frac{M_3}{\left(1 + \frac{\gamma - 1}{2} M_3\right)^{(\gamma+1)/(\gamma-1)}} \frac{\left(\frac{P_4}{P_1}\right)^{(\gamma+1)/2\gamma}}{\left\{\frac{2}{\gamma - 1}\left[\left(\frac{P_4}{P_1}\right)^{(\gamma-1)/\gamma}\frac{\left(1 + \frac{\gamma - 1}{2} M_3^2\right)}{\left(1 + \frac{\gamma - 1}{2} M_3\right)^2} - 1\right]\right\}^{1/2}} \tag{29}$$

Equation (29) is difficult to use; it is easier to select M_3 and A_o/A_p, and then use steady isentropic tables (e.g., Ref. 11) and Eq. (3) to find P_4/P_1. Equation (29) is plotted in Fig. 6 for four area ratios: $A_o/A_p = 1$, .953, .903, and .737. Once the orifice chokes, the pipe flow Mach number is independent of diaphragm pressure ratio and is defined by setting $M_e = 1$ in Eq. (27), i.e., M_3 is found from

$$\frac{A_p}{A_o} = \frac{1}{M_3}\left[\frac{2}{\gamma + 1}\left(1 + \frac{\gamma - 1}{2} M_3^2\right)\right]^{(\gamma+1)/2(\gamma-1)} \tag{30}$$

In Fig. 7, x-t plots are presented which show the effect of the orifice in producing a flow of constant M_3 with choked exit. Throughout this analysis

it has been assumed that the orifice coefficient is one; if there is any contraction in the stream behind the orifice (tank side), the orifice coefficient will be less than unity and the Mach number predicted by the above analysis will be high.

3. EXPERIMENTAL FACILITY

3.1 FACILITY DESIGN

The facility chosen to study the flow produced by a centered expansion wave and its applicability to particle drag studies in the slip flow regime was a pipe 15 ft in length with a 3.1 in. inside diameter. One end of the pipe was open and was attached to an 11 ft^3 dump tank; the other end was closed. A drawing of the facility is presented in Fig. 8. Ordinary water pipe was used and consequently the inside surface was moderately rough; the length of 15 ft was chosen to insure 15 msec of test time. The dump tank was needed because of the pressure level of the experiments, i.e., the tank pressure varied from one mm Hg to a few psi. The inside surface of the tank, which was made of boiler plate, was varnished to eliminate any dirt problem.

A special flange system, machined from steel, was designed so that the pipe and tank could easily be sealed and coupled. One flange screwed directly onto the open end of the pipe to form a flush end surface; this flange had a thickness of .568 in. and an outside radius of 13 in. The other flange, which was welded to the dump tank also had a thickness of .568 in. and a 13-in. outside radius. Its inside radius was 9 in. This was also the size of the hole cut in the tank. A diaphragm to separate the high pressure gas in the pipe from the low pressure gas in the tank was placed

between the flanges, and the pipe and tank were clamped shut with "Vise Grips". The tank was placed on a rolling platform to facilitate closing. To insure a tight seal, an "O" ring was built into the tank flange. A plunger driven forward by a Saval 24 volt D.C. solenoid was used to burst the diaphragm. The orifice plates (machined from aluminum) were attached to the pipe flange with machine screws; the outside diameter of the orifice plates was 5 in. while their thickness was 1/8 in.

3.2 DIAPHRAGM: MATERIAL, ARRANGEMENT AND BREAKER

An extensive study was carried out to determine the combination of diaphragm material, arrangement, and breaker that would yield the best formed expansion wave for diaphragm pressure differences from a few mm Hg to a few psi. It was found that Dupont MD-31 cellophane, 0.001 in. thick, worked best when broken by a sharp compass needle point. The compass needle point was attached to the end of the solenoid driven plunger. For a diaphragm pressure difference of a few mm Hg, it was best to have the unsupported surface area of the diaphragm as large as possible; for the flange arrangement discussed in the preceding section it was possible to expose 63.6 $in.^2$ of diaphragm surface to the pressure difference. When punctured in the center by the compass needle point the cellophane split into several petals along rays 4.5 in. in length. The accelerated gas issuing

from the 1.55 in. radius pipe easily pushed these petals out of the way. Very little shattering of the cellophane occurred with this scheme. At diaphragm pressure differences of a few psi, the diaphragm surface area had to be reduced; otherwise the diaphragm would break before the full pressure difference was reached. As shown in Fig. 8, the exposed area of the diaphragm was reduced to the cross-sectional area of the pipe (3.1 in. diameter) with the aid of an adapter plate attached to the solenoid support in the tank. (When the pipe and tank were sealed, the adapter plate merely pushed against the diaphragm to decrease its unsupported surface.) When broken, the cellophane still petaled but not as neatly as in the low pressure case, and some shattering occurred. However, this method was better than using a thicker cellophane without the adapter plate. Other diaphragm materials tried were .0017 in. cellophane, .0015 in. mylar, and dental dam. The .0017 in. cellophane and mylar were found to be too strong (for the diaphragm pressure differences used) and exhibited erratic breaking characteristics. The dental dam was stretched tightly over the pipe end and broken mechanically; it pulled away from the pipe centerline very quickly but vibrated, causing disturbances in the flow.

Various plunger ends were tried. A blunt end plunger produced many well formed cellophane petals along with some shattering. However, the blunt end plunger had to be discarded because it produced a weak compression system which preceded the expansion wave into the pipe; this was

caused by the blunt plunger first pushing the diaphragm forward before breaking. The compass needle end was used because it eliminated this undesirable effect. A plunger end with crossed knife edges was also tried; however, it gave erratic breaking and did not produce well formed petals.

Tests were conducted with the 24 volt D.C. solenoid supplied with 12, 24, 36, and 48 volts D.C. It was found that it was best to underdrive the solenoid by supplying it with only 12 volts. If the solenoid was operated at higher voltage it also caused a weak compression system to precede the expansion wave in the pipe; this effect occurred even if the compass point was used and intensified with increased supply voltage. The only difficulty encountered by driving the solenoid with only 12 volts was that the time for the solenoid plunger to travel forward varied slightly between runs — with increasing supply voltage, the travel time became very repeatable.

3.3 PRESSURE SYSTEM AND INSTRUMENTATION

In Fig. 9 a diagram of the vacuum and pressure systems is shown; the pressurization system was included so that tests could be conducted with the tank removed. In these tests the pipe could be pressurized to 2.7 atm; .0017 in. cellophane was used for the diaphragm and was broken manually by striking it with a sharp object. Design of the vacuum system was such that both the pipe and tank were evacuated to the desired P_4, and then the tank was evacuated further to P_1. A hard vacuum was unnecessary and

therefore the limit of evacuation was approximately 0.1 mm Hg. Depending upon the range of operation, P_4 and P_1 were read on either of the Wallace and Tiernan absolute pressure gauges or on two mercury manometers. The Wallace and Tiernan gauges were calibrated against a U-tube manometer containing dibutylphthalate.

To measure the flow static pressure, P_3, a 1/8 in. diameter hole was drilled through the pipe wall and a Kistler 701A pressure transducer was mounted on the outside wall. The flow total pressure, P_{3t}, was measured with the aid of an impact tube connected to another pipe-mounted Kistler 701A transducer—see Fig. 10. The impact tubes used had outside diameters of 1/4 in. and 1/8 in. and were made of copper and steel respectively. In Ref. 7 it is indicated that an impact tube yields the correct steady flow total pressure if the Reynolds number based on free stream conditions and tube inside diameter is greater than 60—for the tests conducted this condition was always satisfied. More recent work on the effects of viscosity and slip on the flow near a stagnation point is found in Ref. 8. By using Fig. 7 of this reference, the total pressure reading of the impact tube could be corrected. However, for the tests run, this correction was always negligible, even for the most severe cases, and therefore the impact tube pressure measured was taken to be the correct total pressure.

Again referring to Fig. 10, which shows the complete electrical system, it is seen that two Kistler Model 566 multi-range electrostatic charge

amplifiers were used to amplify the signals from the pressure transducers. This system had a rise time of a few microseconds and was very sensitive to weak pressure signals. The signals from the amplifiers were fed to a dual beam, four channel, Tektronix oscilloscope where the pressure traces were displayed and recorded on Polaroid film. The oscilloscope was triggered externally with the aid of a time delay which was activated when the solenoid was fired. To avoid excessive noise in the pressure traces, 5 megohm resistors were placed in the lines between the transducers and amplifiers. Coupled with the capacitance of the lines, these resistors acted as filters sufficient to eliminate much of the noise caused by mechanical tube vibrations. The response of the transducer-amplifier system to aerodynamic pressure changes was not greatly affected by the inclusion of the filters. Because the activated solenoid produced an electrical field, the pipe (with which the transducers were in electrical contact) had to be isolated from the tank (to which the solenoid was fastened). This was accomplished by covering the outside surface of the pipe flange with a sheet of mylar: when the clamps were applied one end touched the mylar while the other end touched the tank flange. The cellophane diaphragm isolated the inside surfaces of the flanges.

Calibration of the oscilloscope voltage levels was accomplished by comparison with "known" voltage drops as measured by a high accuracy potentiometer. Calibration of the Kistler transducer-amplifier combination was more difficult; this was due to the natural time constant of the Kistler equipment,

i.e., when the Kistler combination was displaced from its tare value, it returned (to tare) naturally according to its time constant. The time constant was measured and its influence was incorporated into the data reduction. As it was of the order of a second, its effect over the time interval examined experimentally (22 msec) was small, but not negligible. The crystals used in Kistler transducers are known to be temperature sensitive; however, it was felt that this effect was unimportant for these experiments because the temperature change across the expansion wave was no larger than $150^{\circ}R$. The amplification of the Kistler combination was measured using a "miniature" expansion tube of length 6 in. which was pressurized to some level above room pressure. When the diaphragm was punctured, the pressure in the tube quickly dropped from the pressurized level to ambient, i.e., the oscillating unsteady wave system in the tube usually damped out in 3 msec. The pressurized level of the tube and ambient pressure were measured with mercury manometers, and were compared against the pressure traces obtained on the oscilloscope.

4. EXPERIMENTAL PROCEDURE, DATA REDUCTION, AND ERROR ANALYSIS

4.1 SCOPE OF EXPERIMENT

The experiment consisted of determining the Mach number of the flow behind the expansion wave and its steadiness with regard to Mach number, Reynolds number, and dynamic pressure. P_4, P_1, P_3, and P_{3t} were measured; the Mach number (by two methods), Re, q_3, u_3, and diaphragm pressure ratio were calculated knowing these pressures. It was also of interest to determine the boundary layer thickness and profile. This was accomplished by moving the impact tube radially. By comparing velocity profiles, it was possible to distinguish between laminar and turbulent boundary layers. For one series of tests a pressure transducer was located 3 ft from the point of diaphragm rupture, and these results were compared with pressure traces taken at the usual position of 9 in. from the diaphragm. This series showed the effect of decreasing test time with increasing distance from the diaphragm rupture point. It was also important to experimentally verify the test time predicted by theory.

The experiments were conducted at Reynolds numbers (based on pipe diameter) of approximately 1.98×10^4 and 1.98×10^5, using four different orifice-to-pipe area ratios, i.e., $A_o/A_p = .737, .903, .953$, and 1. Due to difficulty in measuring the pipe diameter, the tolerance on the area ratios is approximately $\pm .01$. In what follows, Re $\cong 1.98 \times 10^4$ will be

referred to as the low pressure or low Reynolds number case, while $Re \cong 1.98 \times 10^5$ will be referred to as the high pressure or high Reynolds number case. The flow Mach number was varied from 0.2 to 0.9. To eliminate the effect of compression waves issuing from the dump tank, a series of runs was made with the tank removed. This, of course, resulted in higher pressure levels since P_1 had to be room pressure; the Reynolds number ranged from 6.50×10^5 to 1.94×10^6.

4.2 EXPERIMENTAL PROCEDURE AND DATA REDUCTION METHOD

For each run the tank and pipe were pumped to the desired pressures; the tank pressure, P_1, and the pipe pressure, P_4, were read. The diaphragm was burst mechanically, and the resulting expansion wave accelerated the stationary gas. A time history of the static and total pressures, 9 in. from the pipe exit, was taken using the pressure transducer-amplifier-oscilloscope arrangement described in Section 3.3. Typical oscilloscope pressure traces are shown in Fig. 11. As the incident expansion wave moved past the observation point, the static pressure dropped from P_4 to P_3 and the total pressure dropped from P_4 to P_{3t}. The pressure dropped again when the reflected expansion wave passed the pressure sensors. Four measurements were made from Polaroid photographs of the oscilloscope traces. The static and total pressures were measured at 7 and 22 msec after the passage of the head of the expansion wave at the pressure sensors. Measurement of the pressure at these two times was the most meaningful, since

at 7 msec the tail of the incident expansion wave had usually just passed, and at 22 msec the reflected expansion wave was just about to terminate the quasi-steady flow at the observation point. Between 7 and 22 msec the change in static and total pressures was due to second order effects ("tank compressions" and boundary layer) and was usually linear.

For each time of measurement, the flow static pressure and total pressure were determined on the basis of the pressure drops from the oscilloscope traces. The Mach number was computed from the static pressure ratio using the relation

$$M_{3s} = \frac{2}{\gamma - 1}\left[\left(\frac{P_4}{P_3}\right)^{(\gamma-1)/2\gamma} - 1\right] \tag{31}$$

and from the ratio of total pressure to static pressure using the usual relation for steady isentropic flow, i.e.,

$$M_{3t} = \left\{\frac{2}{\gamma - 1}\left[\left(\frac{P_{3t}}{P_3}\right)^{(\gamma-1)/\gamma} - 1\right]\right\}^{1/2} \tag{32}$$

Density and temperature of the gas behind the expansion wave were found using Eq. (4) and (5) respectively, and the speed of sound was found using Eq. (2). Air was used throughout, and it was assumed that $T_4 = 530^{\circ}R$ and $a_4 = 1130.0$ ft/sec.

Equations (31) and (32) show that the experimental value of the flow Mach number could be determined from either of two pressure ratios, P_4/P_3 or

P_{3t}/P_3. As one check on the consistency of the experiment, both methods were used to evaluate the Mach number. Because two Mach numbers were determined, two velocities, dynamic pressures, and Reynolds numbers could also have been determined. However, as explained below in Section 5.2, M_{3t} (determined by P_{3t}/P_3) should be more "correct" than M_{3s} (determined by P_4/P_3), especially at 22 msec. Therefore M_{3t} is taken as the correct value for M_3 while M_{3s} is calculated only for comparison. (It will be shown that from the standpoint of probable error it would be better to take M_{3s} as the correct Mach number.) Therefore, the flow Mach number, velocity, dynamic pressure, and Reynolds number are expressed by

$$M_3 = M_{3t} \tag{33}$$

$$u_3 = M_3 a_3 \tag{34}$$

$$q_3 = (1/2)\,\gamma\, P_3 M_3^{\,2} \tag{35}$$

$$Re = \frac{\rho_3 u_3 d_p}{\mu_3} \tag{36}$$

where μ_3 is found using Eq. (11).

In analyzing the boundary layer growth, it is important to know the distance that the gas has travelled, i.e., the length of the boundary layer. Since the expansion wave is thin at the observation point, for ease of

calculation it has been assumed that the gas is accelerated from zero velocity to u_3 upon the passage of the center of the expansion wave. By definition, the speed of the center of the expansion wave is

$$\frac{x}{t} = a_4 - \frac{\gamma + 1}{4} u_3$$

The time required for the wave center to travel from the observation point to some upstream point X is given as

$$t_1 = \frac{X}{a_4 - \frac{\gamma + 1}{4} u_3}$$

and the time required for the accelerated gas to travel from X to the observation point is given by

$$t_2 = \frac{X}{u_3}$$

Then the distance travelled by the gas is

$$X = \frac{u_3 \left(a_4 - \frac{\gamma + 1}{4} u_3\right)}{\left(a_4 + \frac{3 - \gamma}{4} u_3\right)} (t_1 + t_2)$$

or

$$X = \frac{u_3 \left(a_4 - \frac{\gamma + 1}{4} u_3\right)}{\left(a_4 + \frac{3 - \gamma}{4} u_3\right)} (t_m - t_d/2) \qquad (37)$$

where t_m is the time since the passage of the head of the expansion wave past the observation point, and t_d is the time thickness of the expansion wave at the observation point. Since t_d is small for the Mach numbers of concern here, it can be neglected compared to t_m. The Reynolds number based upon X can now be determined, i.e.,

$$Re_X = \frac{\rho_3 u_3 X}{\mu_3} \tag{38}$$

As a measure of the steadiness of the flow behind the expansion wave, the percentage change per millisecond, g, was calculated for P_3, u_3, M_3, q_3, and Re. In general, the percentage change per millisecond of some quantity s is expressed as

$$g(s) = \frac{\Delta s}{(s)_{ave}} \times \frac{100}{\Delta t} \tag{39}$$

where Δt is the time interval between measurements; e.g., usually Δt = 22 - 7 = 15 msec, since the measurements were made at the beginning and at the end of useful flow period. Δs is the change in s during Δt

$$\Delta s = (s)_f - (s)_i \tag{40a}$$

and $(s)_{ave}$ is the average value of s during Δt

$$(s)_{ave} = \frac{(s)_f + (s)_i}{2} \tag{40b}$$

For example the percentage change per millisecond in P_3 is calculated from the equation

$$g(P_3) = 2 \frac{(P_3)_{22} - (P_3)_7}{(P_3)_{22} + (P_3)_7} \frac{100}{\Delta t}$$

where the respective measurements were made at 7 and 22 msec after the passage of the head of the expansion wave at the observation point.

4.3 ERROR ANALYSIS

The approximate experimental errors that apply to the measurements made in this study were determined to be as follows:

Initial conditions	;	P_4, T_4	1%
Time interval	;	Δt	3%
Pressure changes	;	ΔP_s, ΔP_t	4.5%

The large errors in Δt and the ΔP's were due to the fact that they were measured from the Polaroid photographs where the scale made measurements difficult. Also the pressure measuring instrumentation (Kistler transducers, Kistler amplifiers, and oscilloscope) required five separate calibrations, i.e., Kistler amplification, Kistler time constant, oscilloscope amplification, oscilloscope screen nonlinearity, and oscilloscope gradicule tilt. Since the ΔP's fundamentally control the accuracy of the entire experiment, it is necessary that great care be taken in their measurement. In future work, it would be advantageous to use a more accurate method of determining the ΔP's (or P_3 and P_{3t}).

The above values for the experimental errors were used to determine the probable error of the several quantities computed for these experiments. The general equation for the probable error $\overline{P}(s)$, of the quantity s, is given in Ref. 9. Applied to the present experiments, this equation takes the form

$$\frac{\overline{P}(s)}{s} = \left\{ \left(\frac{1}{s} \frac{\partial s}{\partial P_4} \right)^2 (\delta P_4)^2 + \left(\frac{1}{s} \frac{\partial s}{\partial T_4} \right)^2 (\delta T_4)^2 + \left(\frac{1}{s} \frac{\partial s}{\partial \Delta P_s} \right)^2 (\delta \Delta P_s)^2 \right.$$

$$\left. + \left(\frac{1}{s} \frac{\partial s}{\partial \Delta P_t} \right)^2 (\delta \Delta P_t)^2 \right\}^{1/2} \tag{41}$$

where in general

$$s = s(P_4,\ T_4,\ \Delta P_s,\ \Delta P_t)$$

since P_4, T_4, ΔP_s, and ΔP_t are the only directly measured quantities. The probable errors of the steadiness parameters g(s) were determined from an equation similar in form to Eq. (41). However in this case

$$g = g(s_f,\ s_i,\ \Delta t)$$

where

$$s_f = s_f\ (P_4,\ T_4,\ \Delta P_{sf},\ \Delta P_{tf})$$

$$s_i = s_i\ (P_4,\ T_4,\ \Delta P_{si},\ \Delta P_{ti})$$

so that

$$g = g(P_4,\ T_4,\ \Delta P_{sf},\ \Delta P_{tf},\ \Delta P_{si},\ \Delta P_{ti},\ \Delta t)$$

The resulting probable errors in P_4/P_1 and the flow variables were found to be:

$$\frac{\bar{P}\,(P_4/P_1)}{P_4/P_1} = 6.2\% \qquad \frac{\bar{P}\,(P_3)}{P_3} = 8.4\%$$

$$\frac{\bar{P}\,(u_3)}{u_3} = 8.9\% \qquad \frac{\bar{P}\,(M_3)}{M_3} = 10.9\%$$

$$\frac{\bar{P}\,(M_{3s})}{M_{3s}} = 2.6\% \qquad \frac{\bar{P}\,(q_3)}{q_3} = 14.8\%$$

$$\frac{\bar{P}\,(Re)}{Re} = 12.2\%$$

It is worth noting that the probable error for M_3 is four times that for M_{3s}. In fact, the probable error for M_{3s} is one third that for P_3. This means that errors incurred in the pressure measurements are minimized by the form of the relation between M_{3s} and P_3 and P_4, i.e., M_{3s} depends upon $(P_4/P_3)^{.143}$. Also, one of the major error contributors, ΔP_t, is not needed in the determination of M_{3s}. It would therefore be advantageous, from the standpoint of probable error, to use M_{3s} as the "correct" flow Mach number. Since u_3, q_3, and Re depend upon Mach number this would most likely also decrease their probable errors, and would eliminate the use of an impact tube to measure P_{3t}.

The probable errors in the steadiness parameters were found to be:

$$\frac{\overline{P}\,[g(P_3)]}{g(P_3)} = 2.5 \qquad \frac{\overline{P}\,[g(u_3)]}{g(u_3)} = 8.5$$

$$\frac{\overline{P}\,[g(M_3)]}{g(M_3)} = 17.7 \qquad \frac{\overline{P}\,[g(M_{3s})]}{g(M_{3s})} = 0.8$$

$$\frac{\overline{P}\,[g(q_3)]}{g(q_3)} = 3.5 \qquad \frac{\overline{P}\,[g(Re)]}{g(Re)} = 5.7$$

Note that these probable errors are very large; e.g., the probable error in the steadiness of P_3 is 2.5 times the value indicated by the measurements. It is concluded that a small error in the measurement of a flow variable yields a very large error in the percentage change of that variable. Note, however, that the probable error in the steadiness of M_{3s} is the smallest of all the flow variables. Again it is concluded that, from an error standpoint, it would be advantageous to use M_{3s} as the "correct" flow Mach number.

5. DISCUSSION OF RESULTS

5.1 THE CENTERED EXPANSION WAVE

Examination of the pressure traces of Fig. 11 shows that the centered expansion wave was always well formed at a distance 9 in. from the point of diaphragm rupture. As the diaphragm pressure ratio increased the expansion wave spread. Most of the pressure drop still occurred in a few msec; however, the "tail end" portion of the wave was greatly stretched, even though little pressure drop occurred across this region. As predicted by theory (Fig. 5), this stretching does not become appreciable until the flow Mach number is above approximately 0.75. This is also verified experimentally: in Fig. 12 (M_3 vs. P_4/P_1 for $A_o/A_p = 1$) it is seen that the experimental Mach numbers are substantially below the theory for Mach numbers above 0.75, i.e., the expansion wave has spread to the extent that it did not pass the observation point completely in the allotted time. For $M_3 \gtrsim 0.75$, the spreading is a major contributor in causing the experimental Mach number to fall below theory. For Mach numbers below 0.75, the time length of the wave is only a few msec. The head of the reflected expansion wave always moved past the observation point (9 in. from pipe end) approximately 22 msec after the arrival of the head of the incident expansion wave. Therefore, at least 15 msec of test gas was obtained, and in the lower Mach

number runs this figure was closer to 20 msec. In this study only the last 15 msec of flow was used; this was done to insure that the impact tube obeyed the theories of steady flow.

It is worth noting that the total pressure reached the "behind the wave" value before the static pressure did. Assuming essentially equal response times for the static and total pressure instrumentation, this characteristic indicates that the static pressure is the better indicator of the passage of the expansion wave and the beginning of the useful quasi-steady flow. In the high pressure runs, large amplitude noise was observed in the total pressure traces immediately after the passage of the expansion wave (see Fig. 11). It appears that this noise was due to mechanical vibrations of the impact tube, since it damped out quickly and was more pronounced at higher pressure levels where the impact force was greater. Generally more noise was encountered in the high pressure runs even though the oscilloscope amplitude was decreased linearly.

From pressure traces taken 3 ft upstream from the diaphragm rupture point (Fig. 11-ℓ and 11-m), the time width of the expansion wave was greater than for runs of similar diaphragm pressure ratio taken at 9 in. As P_4/P_1 approaches 3.59 (i.e., the choking condition for no orifice) the widening effect becomes pronounced and very little period of steady flow is obtained. This was expected on the basis of the x-t plot for the unsteady centered expansion wave; e.g., Fig. 2. It is therefore desirable to test as close to the

point of diaphragm rupture as possible. However, because of three dimensional effects, the testing point must be somewhat removed from the pipe exit, especially when exit orifices, which have a significantly smaller diameter than that of the pipe, are used.

5. 2 EXPERIMENTAL MACH NUMBER

The Mach number in the flow behind the centered expansion wave can be determined either from the static pressure ratio across the expansion wave, i. e., P_4/P_3, or by the ratio of total to static pressure behind the wave, i. e., P_{3t}/P_3. For an expansion wave in a shock tube, Glass and Hall (Ref. 10) imply that the isentropic relations between pressure, temperature, and density hold very well across a centered expansion wave, but that the velocity calculated using Eq. (1) does not agree satisfactorily with direct experimental measurements. For this reason the total pressure was measured with the aid of an impact tube positioned along the pipe centerline; and the "correct" value of the experimental Mach number was calculated from

$$M_3 = \left\{ \frac{2}{\gamma - 1} \left[\left(\frac{P_{3t}}{P_3} \right)^{(\gamma-1)/\gamma} - 1 \right] \right\}^{1/2}$$

The "correct" value of the velocity follows using the isentropic definition of the speed of sound, i. e., $a = \sqrt{\gamma RT}$, and the isentropic relation between

temperature and pressure. The above scheme was assumed to give the best results for direct measurement of only P_4, P_3, and P_{3t}. As a comparison the experimental Mach number was also calculated using the static pressure ratio.

In the following discussion M_{3t} is the Mach number based on P_{3t}/P_3, M_{3s} is the Mach number based on P_4/P_3, and both M_{3s} and M_{3t} are determined at 7 and 22 msec after the passage of the head of the expansion wave. From Fig. 16 it is observed that at 7 msec the agreement between M_{3s} and M_{3t} is good, except possibly for the high pressure runs at low Mach numbers. This indicates that immediately behind the expansion wave the unsteady isentropic relation between M_3 and P_4/P_3 also yields the "correct" Mach number; it also indicates that the impact tube obeyed the steady flow relation between M_3 and P_{3t}/P_3. For measurements made at 22 msec, M_{3t} is generally higher than M_{3s}. This result is slightly more pronounced at low Reynolds numbers. Since the impact tube appeared to obey the steady flow relation at 7 msec, and since there were only small variations in the pressure with time behind the expansion wave, M_{3t} is taken as the "correct" Mach number at 22 msec. Using M_{3t} as the "correct" Mach number is further substantiated by the following argument: M_{3s} will yield the correct Mach number only so long as the right running Riemann variable $[\, 2a/(\gamma - 1) + u]$ remains constant; the ideal unsteady theory (and M_{3s}) are based on this fact. However, for a real expansion

tube with an unsteady boundary layer, $[\ 2a/(\gamma - 1) + u\ ]$ is probably not constant. Therefore M_{3s} is probably in error, and M_{3t} is taken as the "correct" value for M_3, and u_3, Re, and q_3 are dependent upon it. In Section 4.3 it was shown that the experimental error for M_{3s} was substantially less than it was for M_{3t}, and therefore it would be advantageous to take M_{3s} as the "correct" Mach number. It appears that this can be done only immediately behind the expansion wave. For consistency in this discussion of results, M_{3t} is taken as the "correct" Mach number at both 7 and 22 msec.

The effect of diaphragm pressure ratio on M_3, for various orifice diameters, is shown in Fig. 12 through 15. These results show that the high Reynolds number Mach numbers are generally below the low Reynolds number values and that this effect increases with decreasing orifice diameter. For 7 msec and pressure ratios near or below 2.5, the experimental Mach number values (M_{3s} and M_{3t}) are near or slightly below the theory; as the orifice diameter is decreased the experimental values move farther below theory. For pressure ratios greater than 2.5, the data at 7 msec is definitely below the theory (except for $A_o/A_p = .903$ at low Reynolds numbers) indicating the effect of an orifice vena contracta (except for $A_o/A_p = 1$ where the spreading of the expansion wave dominates). With $A_o/A_p = .953$, the high Reynolds number points seem to level off to the choked value sooner than the low Reynolds number points do. At high Reynolds numbers with

choked exit, the Mach number appears to be .726 instead of the theoretical value of .776. For $A_o/A_p = .903$ the high Reynolds number case seems to choke at a Mach number of about .63 instead of at the theoretical value of .683 (for some unexplained reason the low Reynolds number points are above theory). Finally for $A_o/A_p = .737$, theory predicts that $M_3 = .492$ for a choked exit, while experimentally the choked values were .41 and .465 for high and low Reynolds numbers respectively. It is difficult to make comparisons concerning the Mach numbers at 22 msec because of the second order effects involved. However, for the intermediate and higher pressure ratios $(M_{3t})_{22}$ was generally the highest experimental Mach number found, and for cases with an orifice it was generally above theory.

One series of tests was made with the dump tank removed; the Mach number was varied from 0.3 to 0.8 and, correspondingly, the Reynolds number varied from 6.50×10^5 to 1.94×10^6. These data are shown in Fig. 17. $(M_{3t})_7$ starts to deviate from theory at a Mach number of approximately 0.5, and $(M_{3t})_7$ is generally near or above $(M_{3s})_7$. $(M_{3t})_{22}$ was the highest data point for $P_4/P_1 \geq 2.0$. These data were not taken at diaphragm pressure ratios high enough to show the effect of wave spreading that is evident in Fig. 12.

The generally good agreement between theory and measurements immediately behind the expansion wave (especially for low pressure ratios and exit diameters near the pipe diameter) indicates that the pipe exit pressure

was very close to P_1, the initial tank pressure. This indicates that any compression system formed by the bursting diaphragm weakened quickly as it spread into the tank; a weakened compression system was compensated for by a strengthened centered expansion wave. Further, no shock wave was ever observed in the pipe. Therefore, as the theory of Section 2.1 assumes, the pressure drop from initial pipe pressure, P_4, to initial tank pressure, P_1, occurs completely across the centered expansion wave. Of course, as gas flows into the tank, its pressure increases slightly above P_1; and this effect must be considered as the expansion wave moves upstream.

5.3 SECOND ORDER EFFECTS

Ideally, the flow behind the centered expansion wave should be steady in all respects. However, due to the action of the rising dump tank pressure and the unsteady boundary layer, variations in the flow behind the expansion wave do occur. After the diaphragm is burst, gas flows into the dump tank causing its pressure to rise. Figure 18 shows that the rise in tank pressure, divided by P_3, is a function of M_3. The gas pressure in the tank becomes greater than the static pressure behind the expansion wave and therefore a weak compression system moves into the pipe. At the observation point, the pressure in the flow behind the expansion wave will increase and the velocity will decrease with time. At the pipe exit, any upstream moving waves have a velocity equal to $(a_e - u_e)$. Therefore, by choking the pipe exit with an orifice the compression system will be eliminated from the pipe.

In Fig. 19, 20, 21, and 22 (which are plots of the rate of change of P_3 and u_3 at the observation point) the effect of the orifice is shown. For decreasing orifice size, which causes choking at a lower flow Mach number, the pressure increase and velocity decrease behind the wave are reduced. However, for choked conditions the flow behind the expansion wave is still not "constant"; there is yet the effect of the unsteady boundary layer. The action of the unsteady boundary layer is more difficult to describe; only the conclusions from the experiments are presented here. For $A_o/A_p = .737$ and flow Mach numbers greater than 0.35, the exit Mach number is choked or very close to being choked; also, the expansion wave remains thin because the maximum flow Mach number attained is 0.5. Therefore, any change in the flow behind the expansion wave should be due to the unsteady boundary layer. Figures 19 to 22 show that the pressure appears to decrease and the velocity appears to increase. This is further substantiated by Fig. 23, which was obtained from data taken with the dump tank removed and without an orifice. The pressure behind the wave only decreases with time, while the velocity increases with time for $M_3 > .54$. However, for $M_3 < .54$ the velocity decreases with time, and this prevents a generalization that the unsteady boundary layer causes the pressure to decrease and the velocity to increase.

Neglecting the decreasing velocity of Fig. 23, it might be possible to conclude that the unsteady boundary layer effect, as observed 9 in. from

the pipe exit, causes a weak unsteady expansion system similar to that of the primary expansion wave with the result that the right running Riemann variable $[2a/(\gamma - 1) + u]$ remains constant throughout the flow. In the previous section, it was shown that this approach is probably in error since $(M_{3t})_{22} > (M_{3s})_{22}$. The change in the total pressure, not shown in the figures, was close to zero for the "no tank" runs, and for the tests with the tank attached and $A_o/A_p = .737$ the value of $g(P_{3t})$ was approximately .1. (For the three larger orifices $g(P_{3t}) \cong .3$.) For a left running expansion system the total pressure should decrease with time; therefore some further doubt is indicated in assuming that the unsteady boundary layer causes an effect similar to that of an unsteady expansion wave. Because $g(P_{3t}) \cong 0$ for the tests where the rising tank pressure was a small influence or no influence at all, the boundary layer effect may cause the main flow (with transformed coordinates) to act as a subsonic steady flow through a converging nozzle. However, the decreasing velocity of Fig. 23 is still unexplained. It appears that the influence of the unsteady boundary layer is complex and simplifying assumptions such as constant mass flow and/or $[u + 2a/(\gamma - 1) = \text{constant}]$ will generally not suffice. However, it seems reasonable to assume that the boundary layer affects the flow more as a steady subsonic area reduction than as an unsteady expansion.

For runs where the orifice diameter is significantly smaller than the pipe diameter, there will probably be some deformation of the centered

expansion wave. As the expansion wave passes through the orifice it will spread and develop a concave curvature, thereby directing more gas towards the centerline of the pipe. To turn the flow streamlines parallel to the pipe wall, a second expansion system following the primary expansion wave is needed. Such a system might have occurred for $A_o/A_p = .737$; however, its effect is indistinguishable from that of the unsteady boundary layer. It should also be remembered that for $M_3 \geq .75$, the primary centered expansion wave is significantly wide, so that any measurement of ΔP_3 or Δu_3 will include this influence.

5.4 APPLICATION TO PARTICLE DRAG STUDIES

Figures 19 through 22 show that as $A_o/A_p \rightarrow 1$, the Mach number for zero change in P_3 and u_3 increases; this is due to the variation in exit conditions. The conditions for zero change in Mach number, Reynolds number, and dynamic pressure over the test gas region can also be found. It should be remembered that M_3, Re, and q_3 are the important parameters for particle drag studies. In Figures 24 and 25, M_3 versus A_o/A_p is plotted for zero change in P_3, u_3, M_3, Re, and q_3 for low and high Reynolds numbers respectively. It is instructive to note that the important parameters do not have coinciding curves of zero change; thus it is impossible to obtain "steady" flow with respect to all of the important parameters simultaneously.

In Fig. 26 and 27, the operating ranges of the expansion tube are shown for the cases of low and high Reynolds numbers, respectively. The operating range is defined as that region where neither M_3, Re, nor q_3 has a percentage

change greater than $\pm$ 3% during the 15 msec period of quasi-steady flow. (It is assumed that a $\pm$ 3% change in the important parameters is tolerable in particle drag studies.) The operating ranges for low and high Reynolds numbers differ somewhat: the operating range for the low pressure case extends from $M_3 = 0$ to $M_3 = .71$, while the operating range for the high pressure case extends from $M_3 = .24$ to $M_3 = .65$. In both cases the orifice-to-pipe area ratios needed range from $A_o/A_p = .65$ to $A_o/A_p = 1$. The reasons for the multivalued shape of the - 3% boundaries for the high Reynolds number case (Fig. 27) are not known. However, it is suspected that the shape of these boundaries have been influenced by the large noise levels occurring at the high pressure condition and the boundary layer transition that occurs during these tests at these conditions.

5.5 BOUNDARY LAYER PROFILE

Figure 28 shows boundary layer profiles that were determined at four values of Re_X by varying the radial location of a 1/8 in. O.D. impact tube. The two lower values of Re_X correspond to $Re \cong 1.98 \times 10^4$ at measurement times of 7 and 22 msec, while the two higher Re_X's have a similar correspondence to $Re \cong 1.98 \times 10^5$. The essential difference between the profiles at 7 and 22 msec is that X increases by a factor of 3: for 7 msec, X is approximately 2.5 ft, while at 22 msec, X is approximately 7.85 ft. For all four profiles, the Mach number of the flow outside of the boundary layer was approximately 0.8. For particle drag studies it is essential to have a central core free of any boundary layer. For a tube 3.1 in. in diameter,

a central core diameter equal to one half the tube diameter appears acceptable. On the basis of Fig. 28, it appears that the low pressure runs satisfy this criterion. At high pressures, it is doubtful that this criterion is exactly satisfied. The velocity profiles indicate that the boundary layer has become turbulent between $Re_x = 6.67 \times 10^5$ and $Re_x = 5.70 \times 10^6$. The two lowest Reynolds number velocity profiles definitely indicate a laminar boundary layer. For $Re_x = 5.70 \times 10^6$, the boundary layer is definitely turbulent: the velocity gradient is large near the wall, but the velocity does not reach the central core value until $r/r_p = 0.3$. Further, it is felt that the total pressure trace of Fig. 11-n clearly shows boundary layer transition at $Re_x \cong 1.9 \times 10^6$. In this run, the impact tube was positioned such that boundary layer transition would be accompanied by a drop in total pressure. Further experiments were carried out in this region and the point of transition (total pressure drop) always occurred between $Re_x \cong 1.9 \times 10^6$ and $Re_x \cong 2.6 \times 10^6$. This is within the range of transition on flat plates and wings as given in Ref. 5.

The boundary layer data obtained in this investigation were insufficient to permit a detailed analysis of the unsteady boundary layer in the expansion tube. However, the data were sufficient to show that, for the operating conditions of interest, the boundary layer was significant and was becoming thick enough to leave an insufficient central core for aerodynamic testing. The pipe used in these experiments had a rough inside surface; this undoubtedly hastened

the transition and the subsequent thickening of the boundary layer. In any case, these data have shown that the boundary layer must be considered in the design and operation of an expansion tube for aerodynamic testing, especially at the low pressures necessary for the particle drag studies.

6. CONCLUSIONS

This study was undertaken in an effort to determine the usefulness of an expansion tube for particle drag studies in the slip flow regime. For the desired range of flow Reynolds numbers and Mach numbers and the tube length used, a quasi-steady flow of at least 15 msec was obtained and in many cases 20 msec was possible. The centered expansion wave always appeared to be well formed at a distance 9 in. upstream from the diaphragm. Weak secondary wave systems appeared to be produced in the flow behind the expansion wave. One system was produced by the rising tank pressure and appeared compressive; a second weak system was produced by the unsteady boundary layer and in many respects appeared to be expansive. By balancing the apparently opposite effects of rising tank pressure and unsteady boundary layer, the conditions for zero change in the important flow variables were obtained.

For particle drag studies the important flow parameters are Mach number, Reynolds number, and dynamic pressure; it was found that zero change in each of these parameters over the last 15 msec of quasi-steady flow could be obtained by using suitable exit orifices. If a maximum change of $\pm$ 3% in 15 msec was allowed in the important drag parameters, the Mach number range for a particle Reynolds number* of 100 was 0 to .71,

*Based on a particle diameter of 1/64 in.

and for a particle Reynolds number of 1000 it was . 24 to . 65. At the higher Reynolds number, the unsteady boundary layer in the tube appeared turbulent and was growing rapidly with time; its thickness was great enough to seriously limit the size of inviscid central core available for aerodynamic testing. At the lower Reynolds number, the boundary layer appeared laminar and was not seriously limiting the central core. However, the results clearly indicated the need to consider the unsteady boundary when designing and operating an expansion tube at pressures low enough for low Reynolds number particle drag research where relatively long periods of quasi-steady flow are desired.

This study has shown that the subsonic expansion tube can provide a quasi-steady flow of sufficient steadiness and length to be useful in "free trajectory" studies of particle drag under conditions of compressible slip-flow. Although the present study was limited to flow times of about 15 msec, it appears that appreciably longer flow times can be obtained by using longer and larger diameter (to accomodate the increased boundary layer thickness) tubes. Actual testing in an expansion tube facility must be preceeded by a detailed calibration to establish the orifice-to-pipe diameter ratio, Mach number, Reynolds number combinations necessary for suitably steady flow and to establish the extent of the inviscid central core at each test condition.

REFERENCES

1. "Dynamics of Two-Phase Flow in Rocket Nozzles," Fourth Quarterly Technical Progress Report, 26 May 1962, United Technology Corporation, Contract No. NOW-61-0760-C.

2. Selberg, B. P., "Shock Tube Determination of the Drag Coefficient of Small Spherical Particles," NASA CR-418, 1965.

3. Liepmann, H. W. and Roshko, A., Elements of Gas Dynamics, John Wiley and Sons, Inc., 1957.

4. Hilsenrath, J., Beckett, C. W., et al., Tables of Thermal Properties of Gases, National Bureau of Standards Circular 564, 1955.

5. Schlichting, H., Boundary Layer Theory, Trans. by J. Kestin, McGraw-Hill Book Co., Inc., 1960.

6. Courant, R. and Friedrichs, K. O., Supersonic Flow and Shock Waves, Interscience Publishers, Inc., 1948.

7. Goldstein, S., Modern Developments in Fluid Dynamics, Vol. 1, Oxford University Press, 1938.

8. Lin, T. C. and Schaaf, S. A., "Effect of Slip on Flow Near a Stagnation Point and in a Boundary Layer," NACA TN 2508, 1951.

9. Beers, Y., Introduction to Theory of Error, Addison-Wesley Publishing Co., 1957.

10. Glass, I. I. and Hall, G., Handbook of Supersonic Aerodynamics, Shock Tubes, Navord Report 1488, Vol. 6, Section 18, Bureau of Ordnance, Department of Navy, 1959.

11. Ames Research Staff, "Equations, Tables, and Charts for Compressible Flow," NACA Report 1135, 1953.

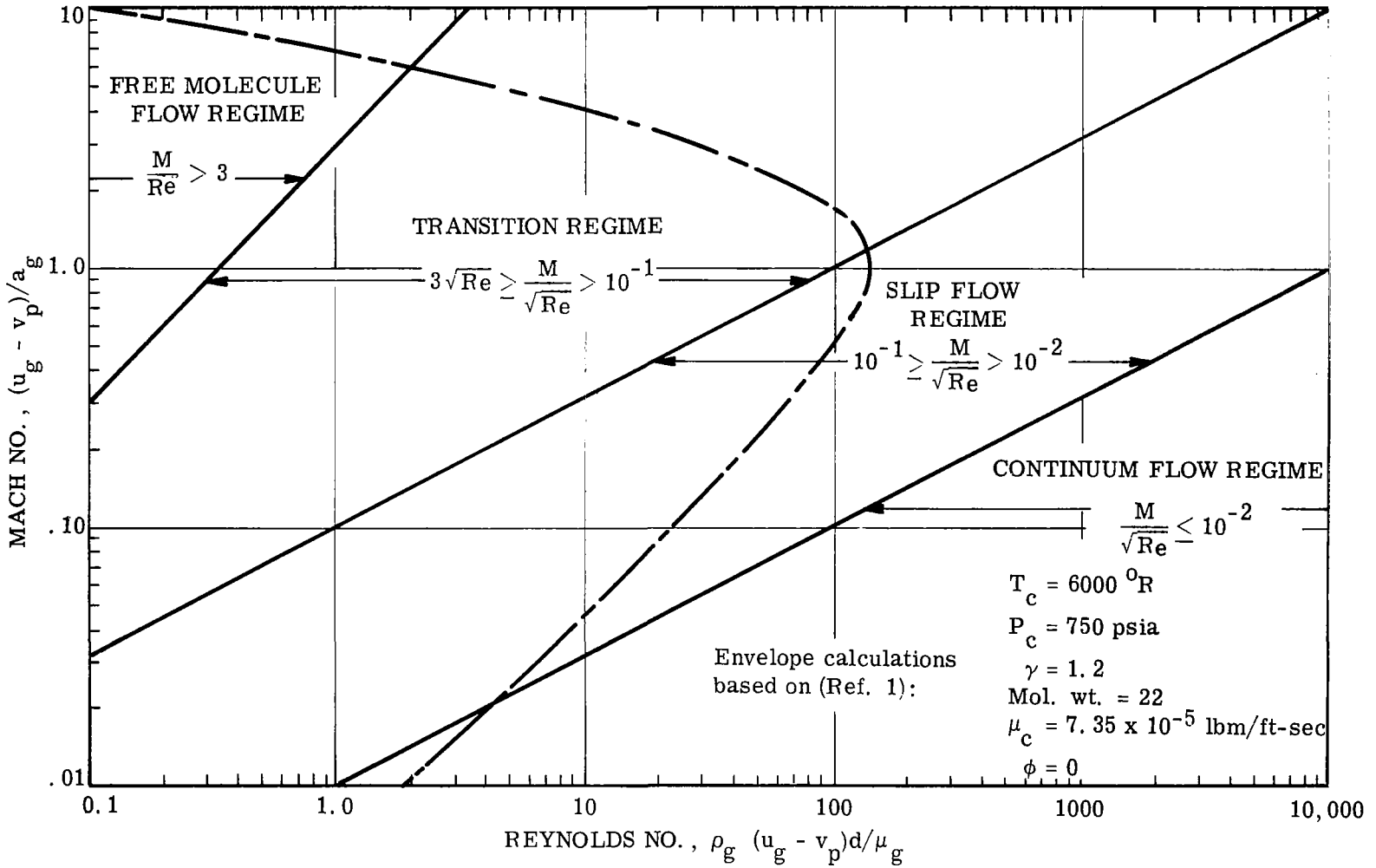

Figure 1. Mach No. - Reynolds No. Flow Regimes Encountered by a Five-Micron Particle in a Rocket Nozzle.

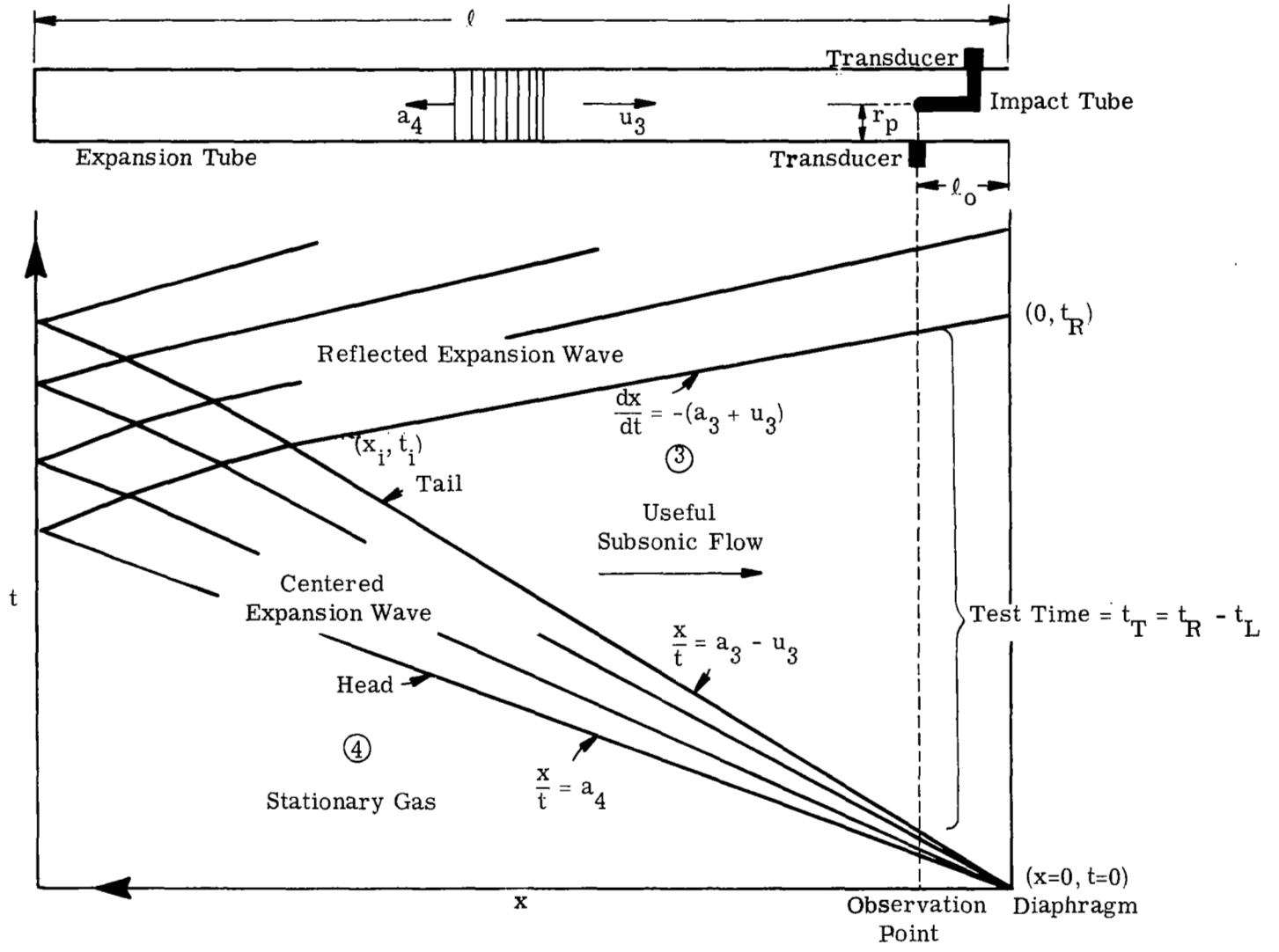

Figure 2. Wave Diagram for Subsonic Expansion Tube (x vs. t).

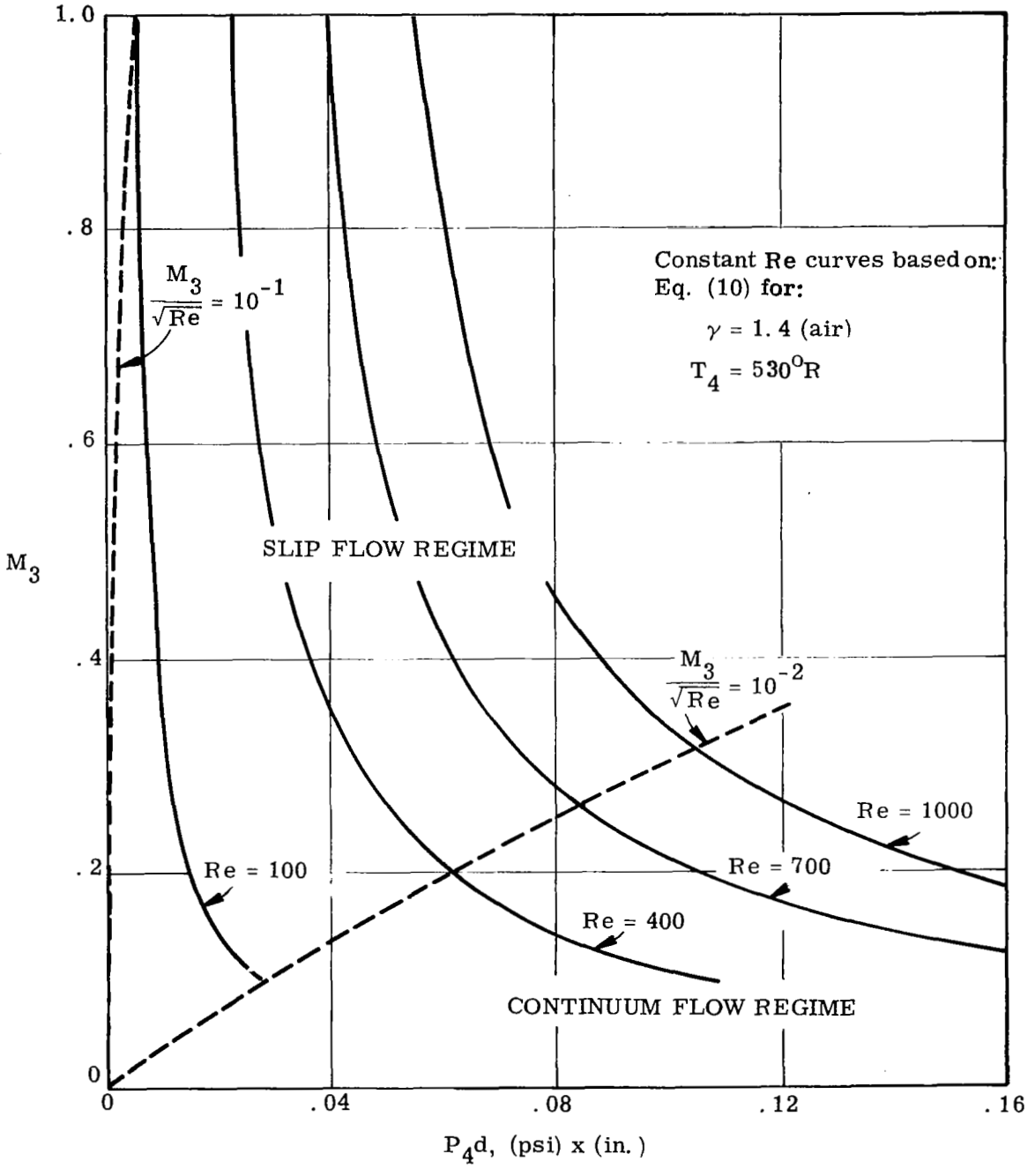

Figure 3. Theoretical Operating Range of Expansion Tube For Particle Drag Studies (M_3 vs. P_4d).

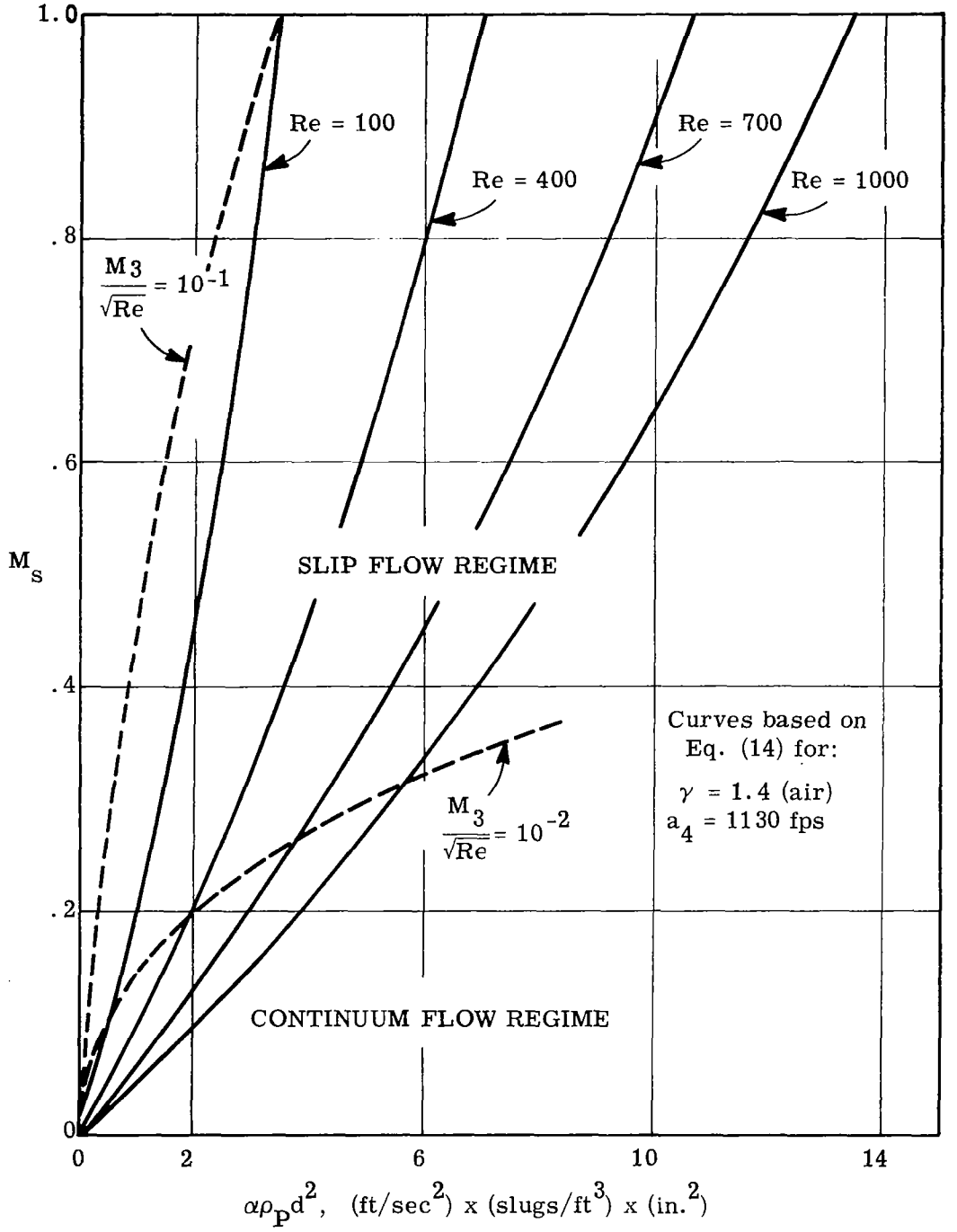

Figure 4. Theoretical Operating Range of Expansion Tube for Particle Drag Studies (M_3 vs $\alpha\rho_p d^2$)

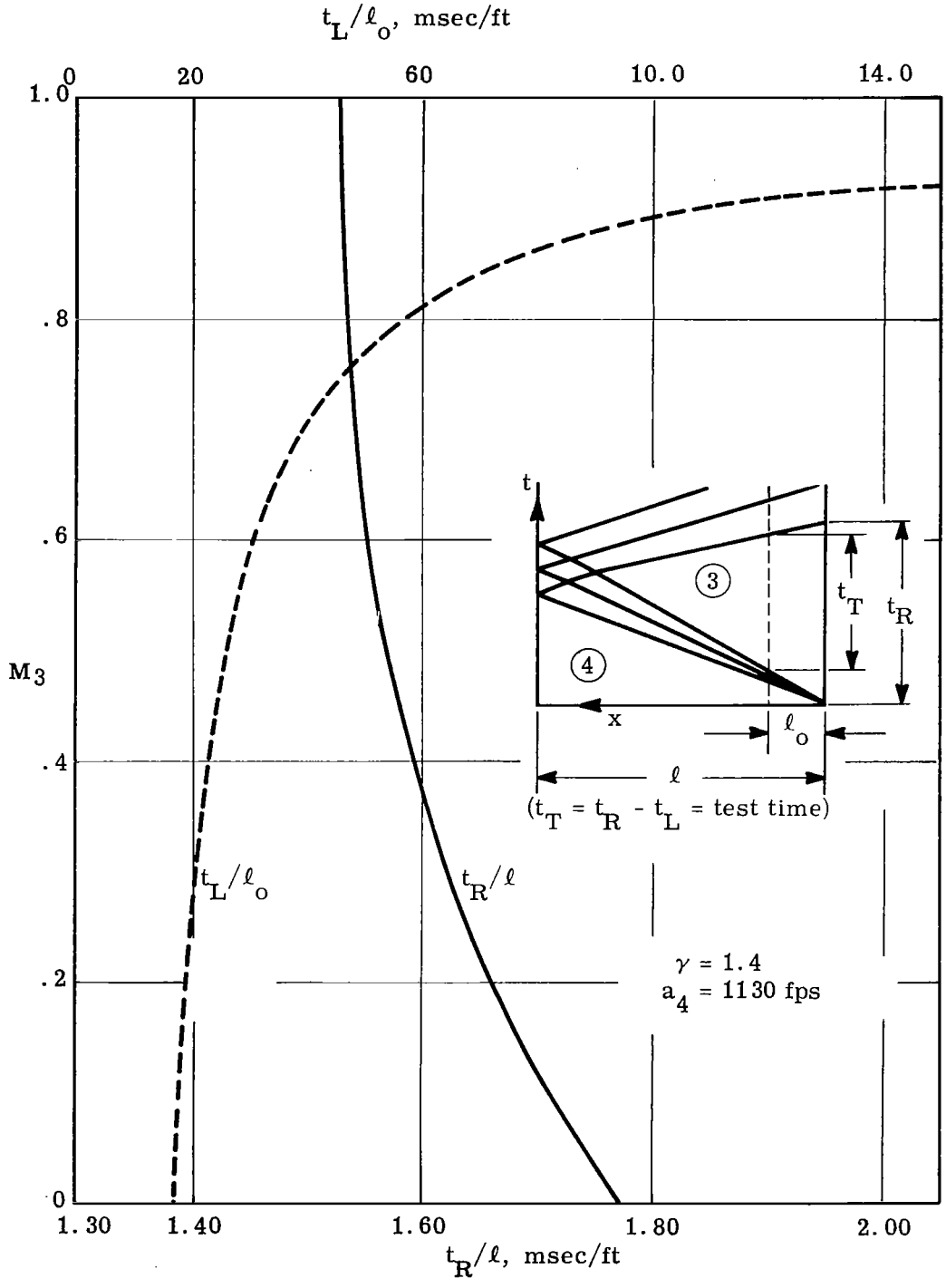

Figure 5. Theoretical Test Time of Expansion Tube.

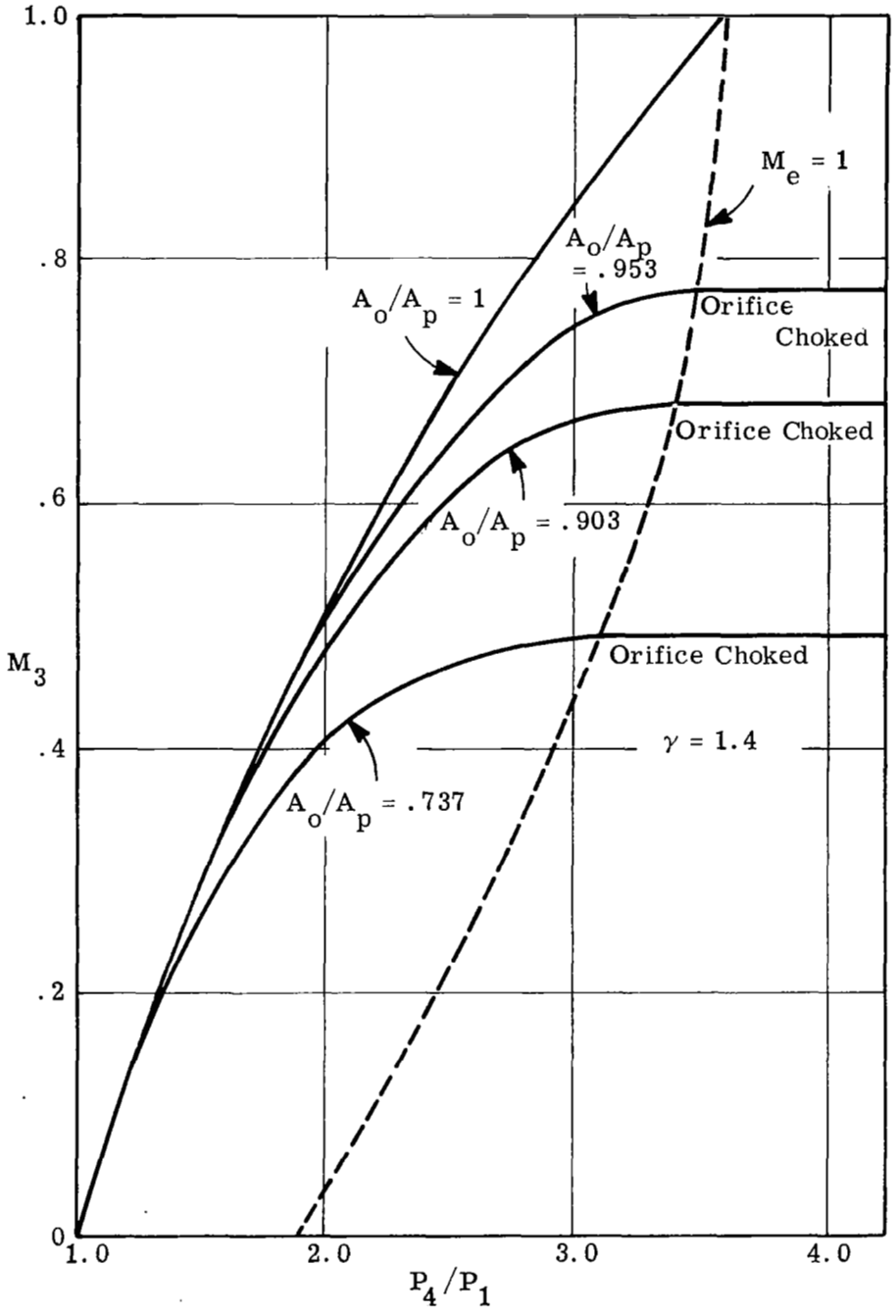

Figure 6. Theoretical Flow Mach Number.

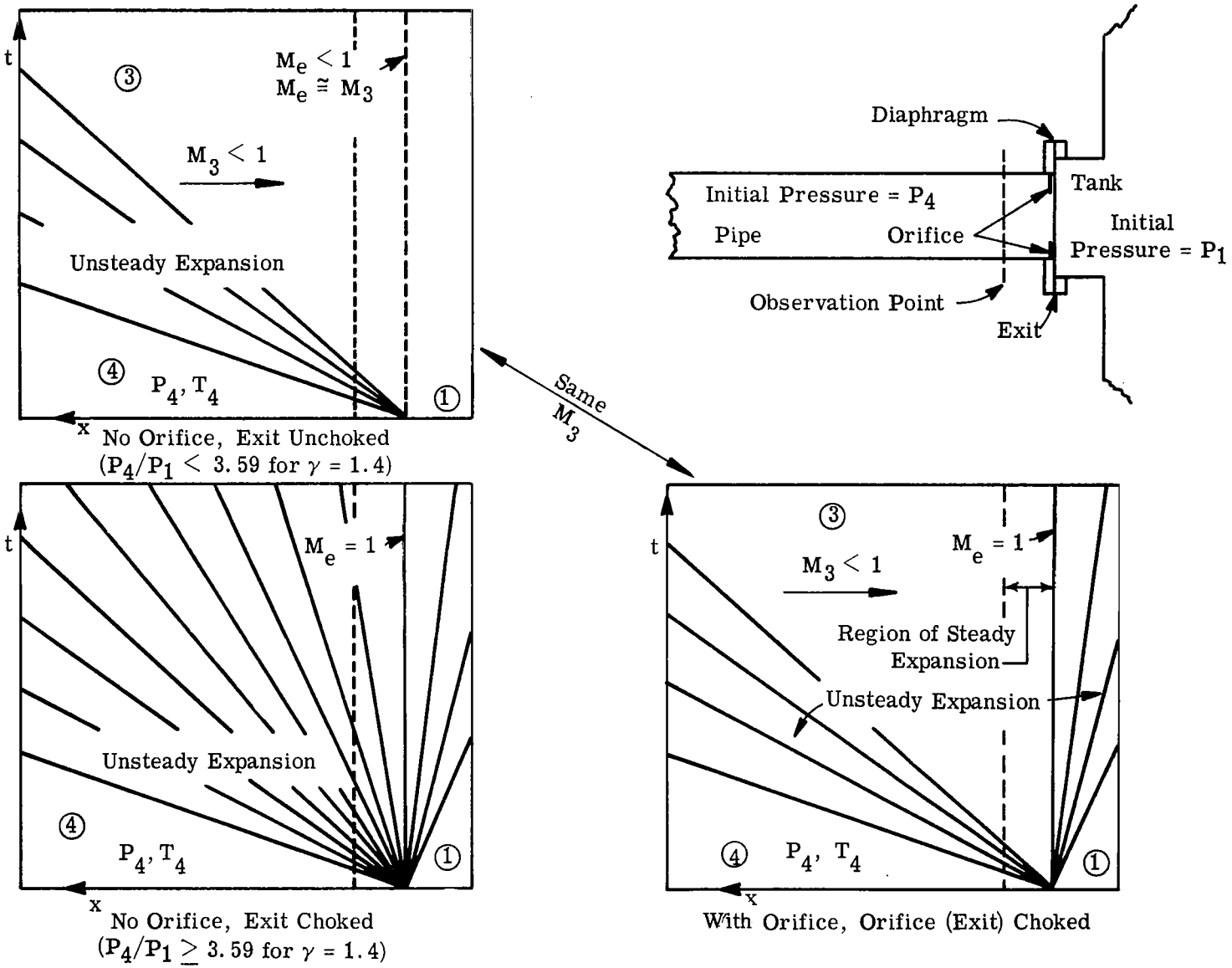

Figure 7. Effect of Tube Orifice Shown by x-t Plots.

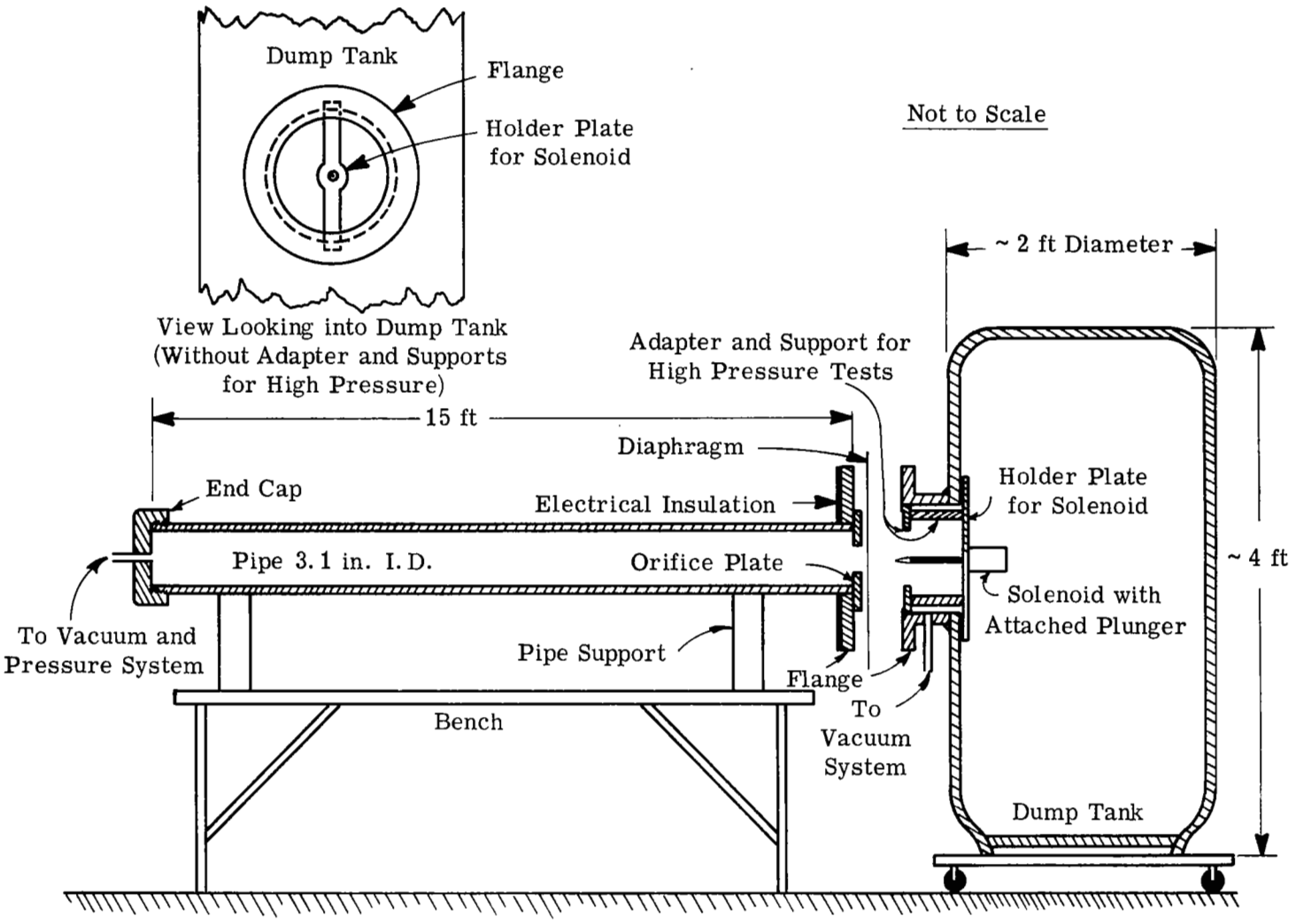

Figure 8. Expansion Tube with Dump Tank.

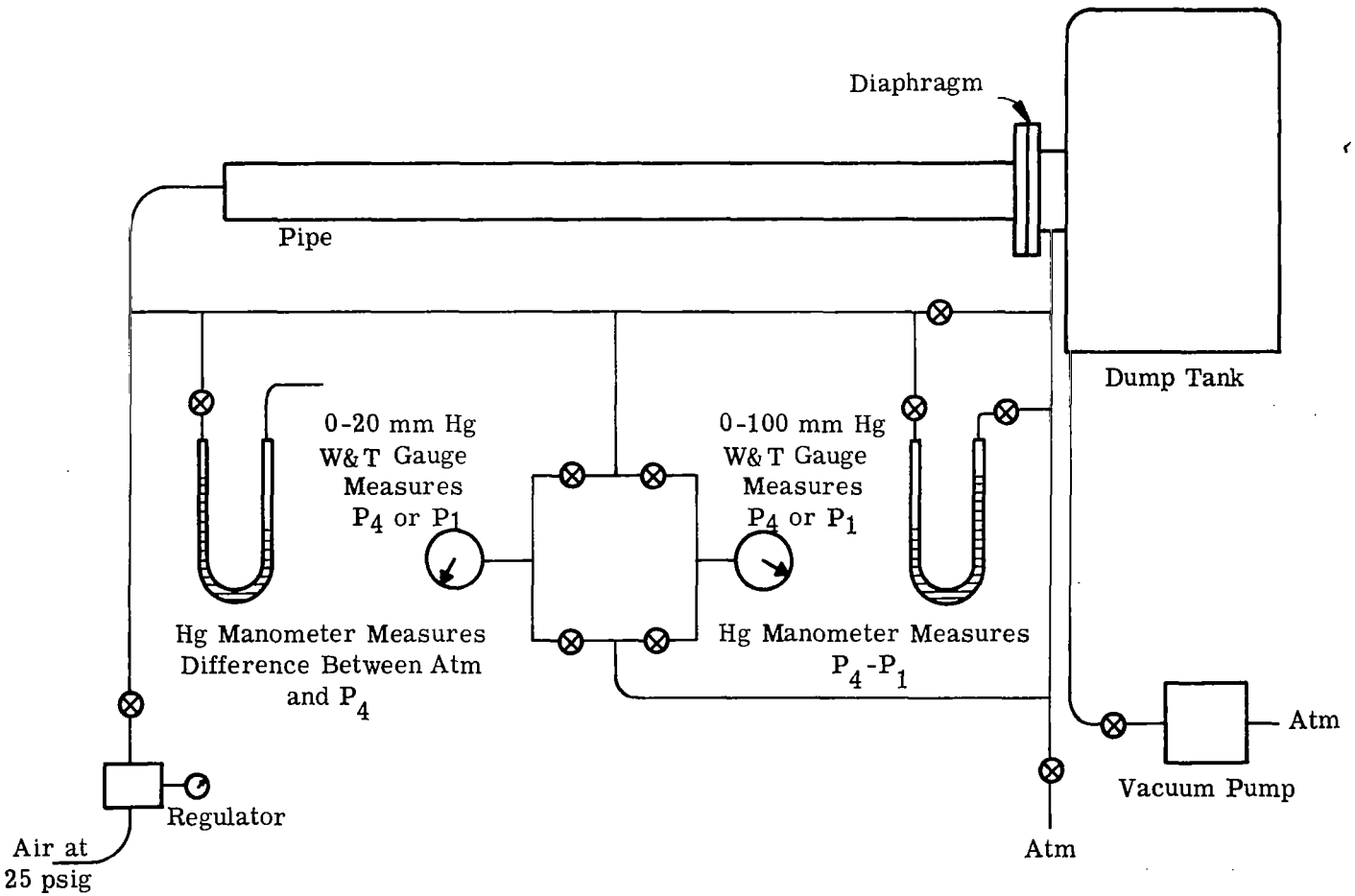

Figure 9. Schematic Diagram of Vacuum and Pressurization System.

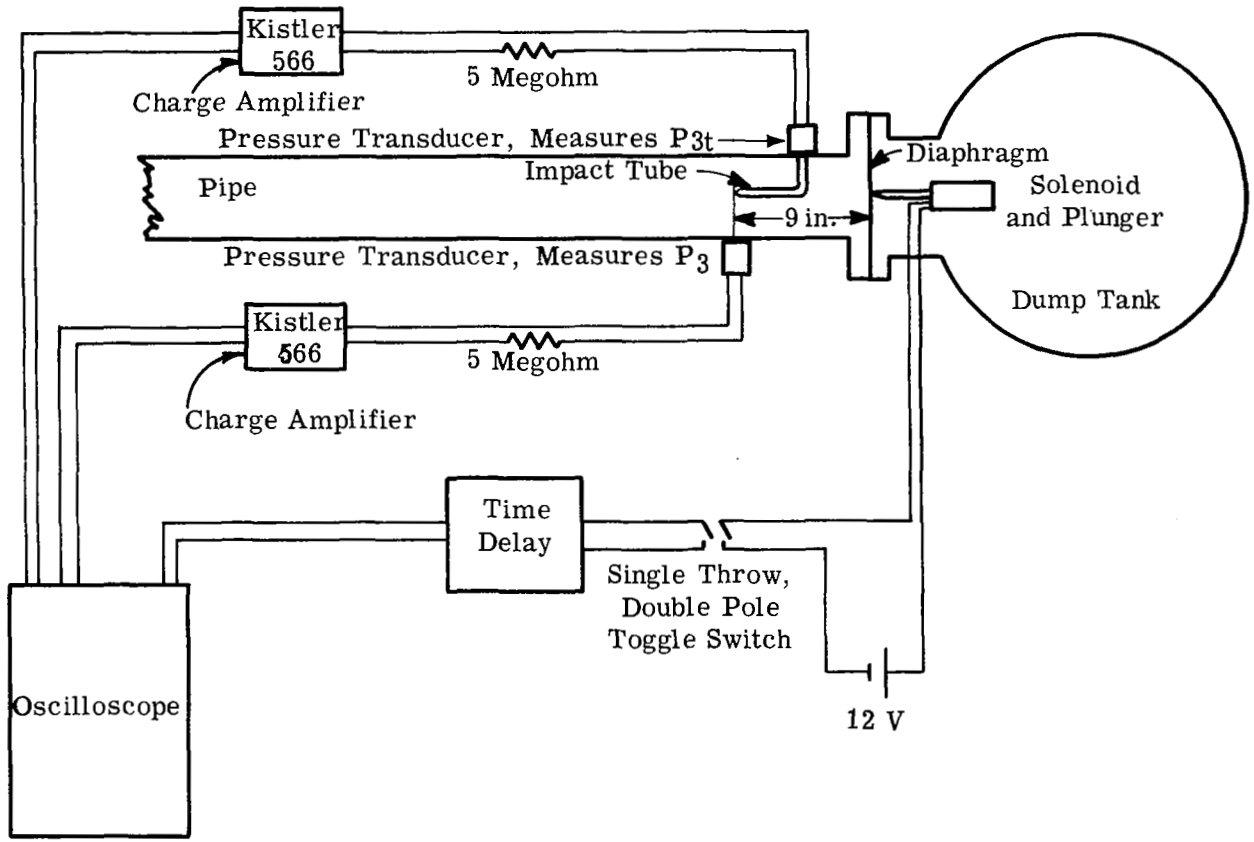

Figure 10. Schematic Diagram of Electrical System.

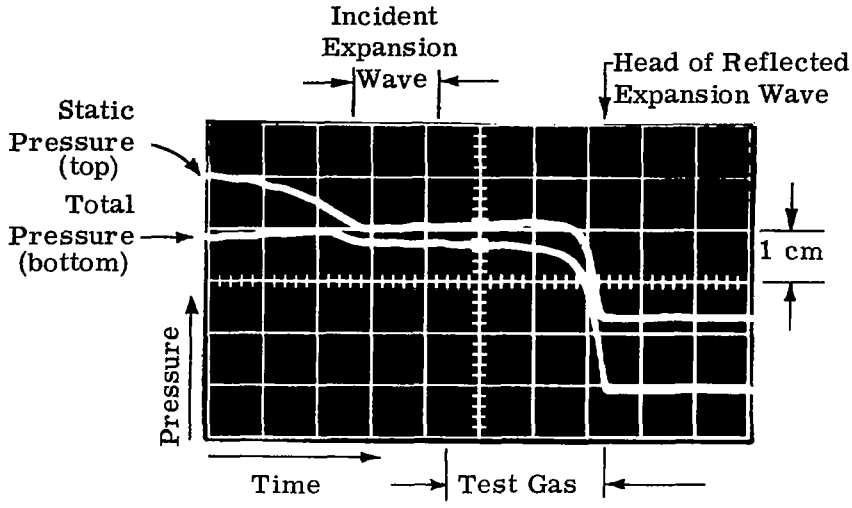

This polaroid photograph of a pair of typical pressure traces is presented as a guide to the following pictures. The labels shown here hold for the entire set of pictures (except that in Figures 11-ℓ and 11-m both traces are of static pressure). Except for Figures 11-ℓ and 11-m all traces taken 9" upstream from diaphragm.

Figure 11-a-Oscilloscope Pressure Traces (Guide)

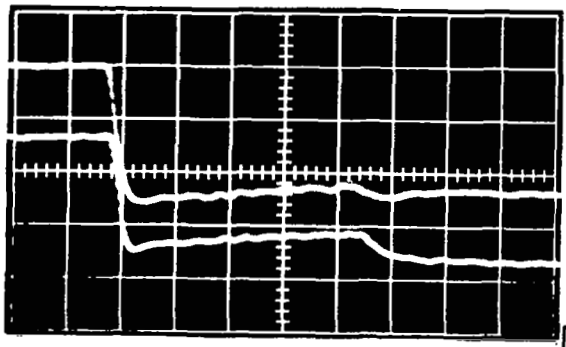

P_4 = 31.04 mm Hg, P_1 = 18.05 mm Hg
P_4/P_1 = 1.720; No Orifice
~.1 psi/cm, 5 msec/cm
$M_3 \cong .4$, $Re \cong 1.98 \times 10^4$
← Figure 11-b

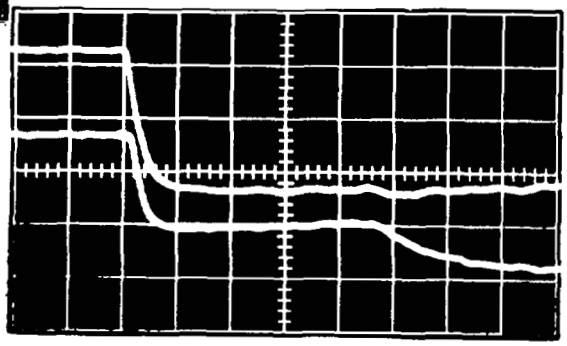

P_4 = 21.04 mm Hg, P_1 = 6.37 mm Hg
P_4/P_1 = 3.303; No Orifice
~.1 psi/cm, 5 msec/cm
$M_3 \cong .825$, $Re \cong 1.98 \times 10^4$
Figure 11-c →

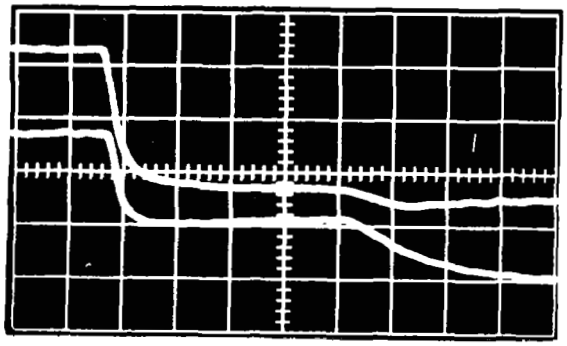

P_4 = 19.87 mm Hg, P_1 = 4.08 mm Hg
P_4/P_1 = 4.870; No Orifice
~.1 psi/cm, 5 msec/cm
Exit Choked, $Re \cong 1.98 \times 10^4$
← Figure 11-d

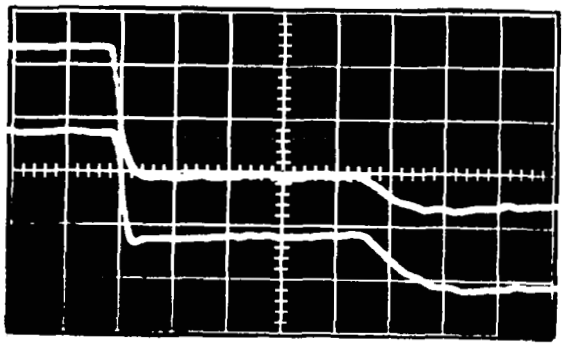

P_4 = 31.65 mm Hg, P_1 = 14.85 mm Hg
P_4/P_1 = 2.131; 2.662" dia. Orifice
~.1 psi/cm, 5 msec/cm
$M_3 \cong .4$, $Re \cong 1.98 \times 10^4$
Figure 11-e →

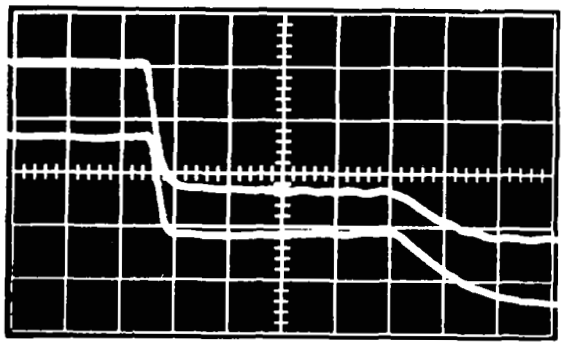

P_4 = 26.07 mm Hg, P_1 = 7.54 mm Hg
P_4/P_1 = 3.458; 2.662" Dia. Orifice
~.1 psi/cm, 5 msec/cm
$M_3 \cong .495$ (orifice choked), $Re \cong 1.98 \times 10^4$
← Figure 11-f

Figure 11(b-f) - Oscilloscope Pressure Traces (Low Pressure)

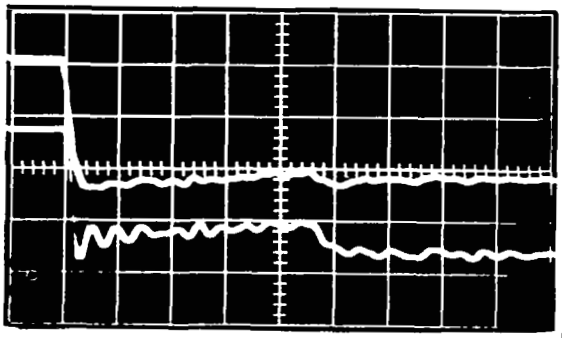

P_4 = 11. 64 in Hg, P_1 = 6. 64 in Hg
P_4/P_1 = 1. 753; No Orifice
~1. 0 psi/cm, 5 msec/cm
$M_3 \cong .4$, $Re \cong 1.98 \times 10^5$
← Figure 11-g

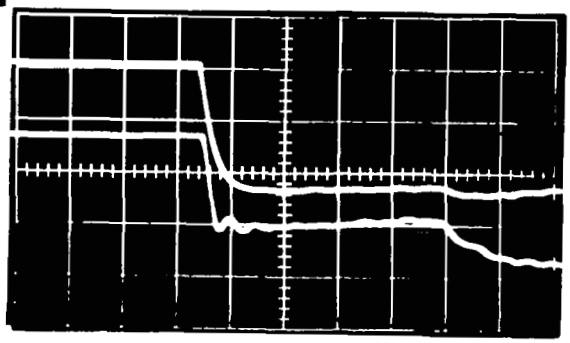

P_4 = 7. 74 in Hg, P_1 = 2. 35 in Hg
P_4/P_1 = 3. 294; No Orifice
~1. 0 psi/cm, 5 msec/cm
$M_3 \cong .81$, $Re \cong 1.98 \times 10^5$
Figure 11-h →

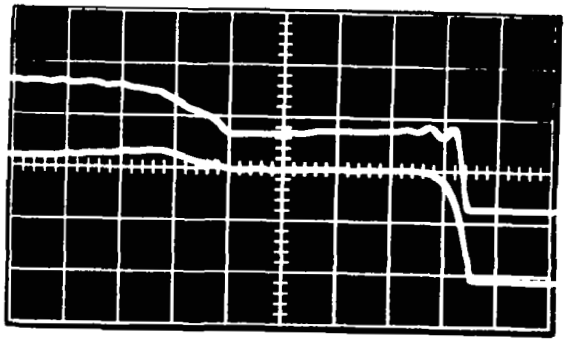

P_4 = 6. 69 in Hg, P_1 = 1. 36 in Hg
P_4/P_1 = 4. 919; No Orifice
~1. 0 psi/cm, 5 msec/cm
Exit choked, $Re \cong 1.98 \times 10^5$
← Figure 11-i

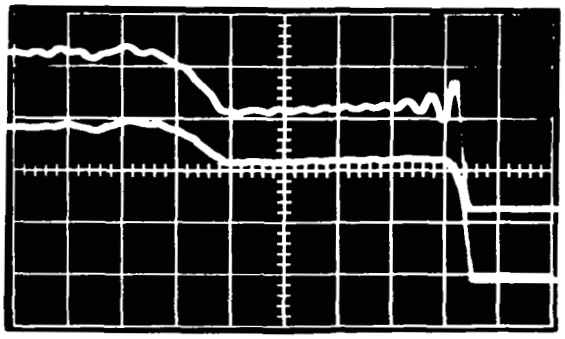

P_4 = 11. 93 in Hg, P_1 = 5. 16 in Hg
P_4/P_1 = 2. 312; 2. 662" Dia. Orifice
~1. 0 psi/cm, 5 msec/cm
$M_3 \cong .375$, $Re \cong 1.98 \times 10^5$
Figure 11-j →

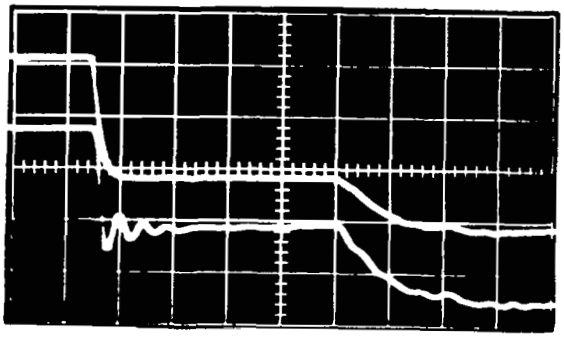

P_4 = 10. 65 in Hg, P_1 = 3. 12 in Hg
P_4/P_1 = 3. 414; 2. 662" Dia. Orifice
~1. 0 psi/cm, 5 msec/cm
$M_3 \cong .44$ (orifice choked), $Re \cong 1.98 \times 10^5$
← Figure 11-k

Figure 11 (g-k) - Oscilloscope Pressure Traces (High Pressure)

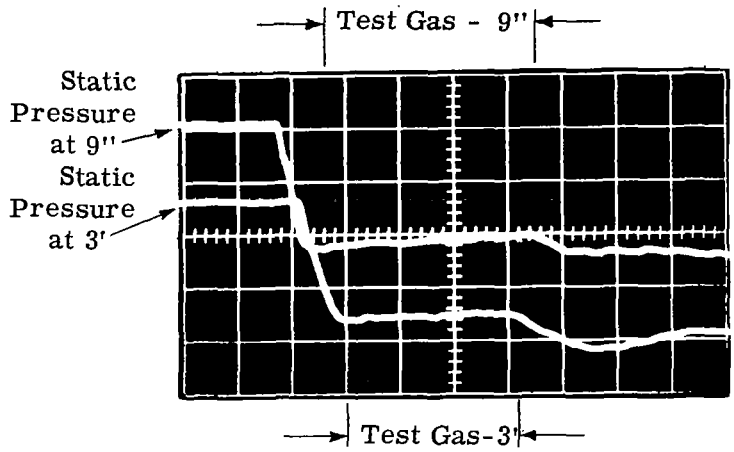

$P_4 = 31.55$ mm Hg, $P_1 = 18.02$ mm Hg

$P_4/P_1 = 1.751$; No Orifice

~. 1 psi/cm, 5 msec/cm

$M_3 \cong .41$, $Re \cong 1.98 \times 10^4$

Top Trace: Transducer 9" From Diaphragm

Bottom Trace: Transducer 3' From Diaphragm

← Figure 11-ℓ

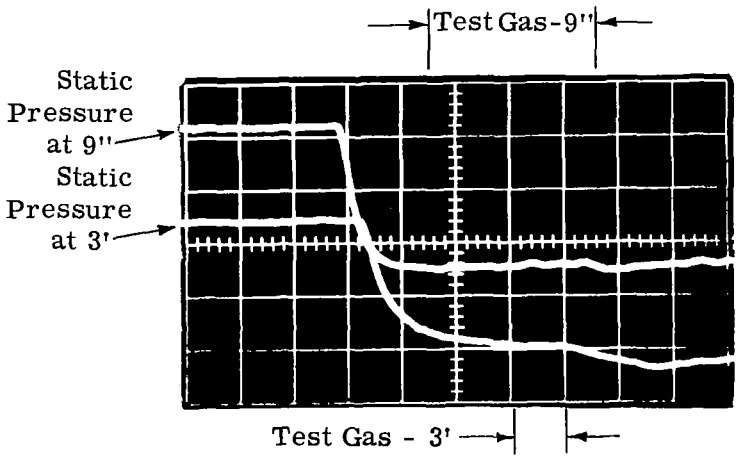

$P_4 = 21.30$ mm Hg, $P_1 = 6.50$ mm Hg

$P_4/P_1 = 3.277$; No Orifice

~. 1 psi/cm, 5 msec/cm

$M_3 \cong .825$, $Re \cong 1.98 \times 10^4$

Top Trace: Transducer 9" From Diaphragm

Bottom Trace: Transducer 3' From Diaphragm

← Figure 11-m

Figure 11(l-m) - Oscilloscope Pressure Traces
(Comparison Between Transducer Locations)

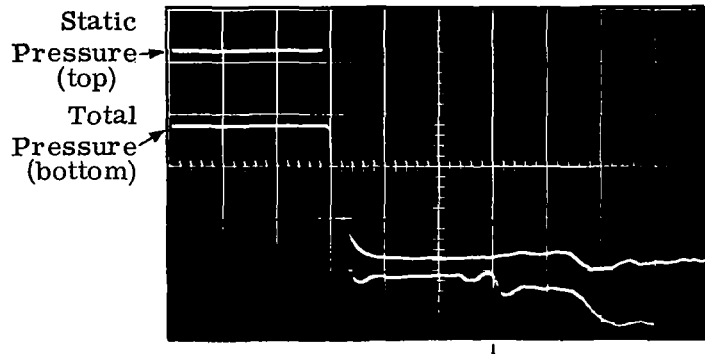

P_4 = 5. 285 in Hg, P_1 = 41. 61 mm Hg

P_4/P_1 = 3. 22; No Orifice

~. 4 psi/cm, 5 msec/cm

M_3 = . 717, Re = 1. 39 x 10^5

1/8" O. D. Impact Tube ~ 1/4" From Wall

$(Re_X)_{trans.} \cong 1.9 \times 10^6$

Figure 11-n - Oscilloscope Pressure Traces
(Boundary Layer Transition)

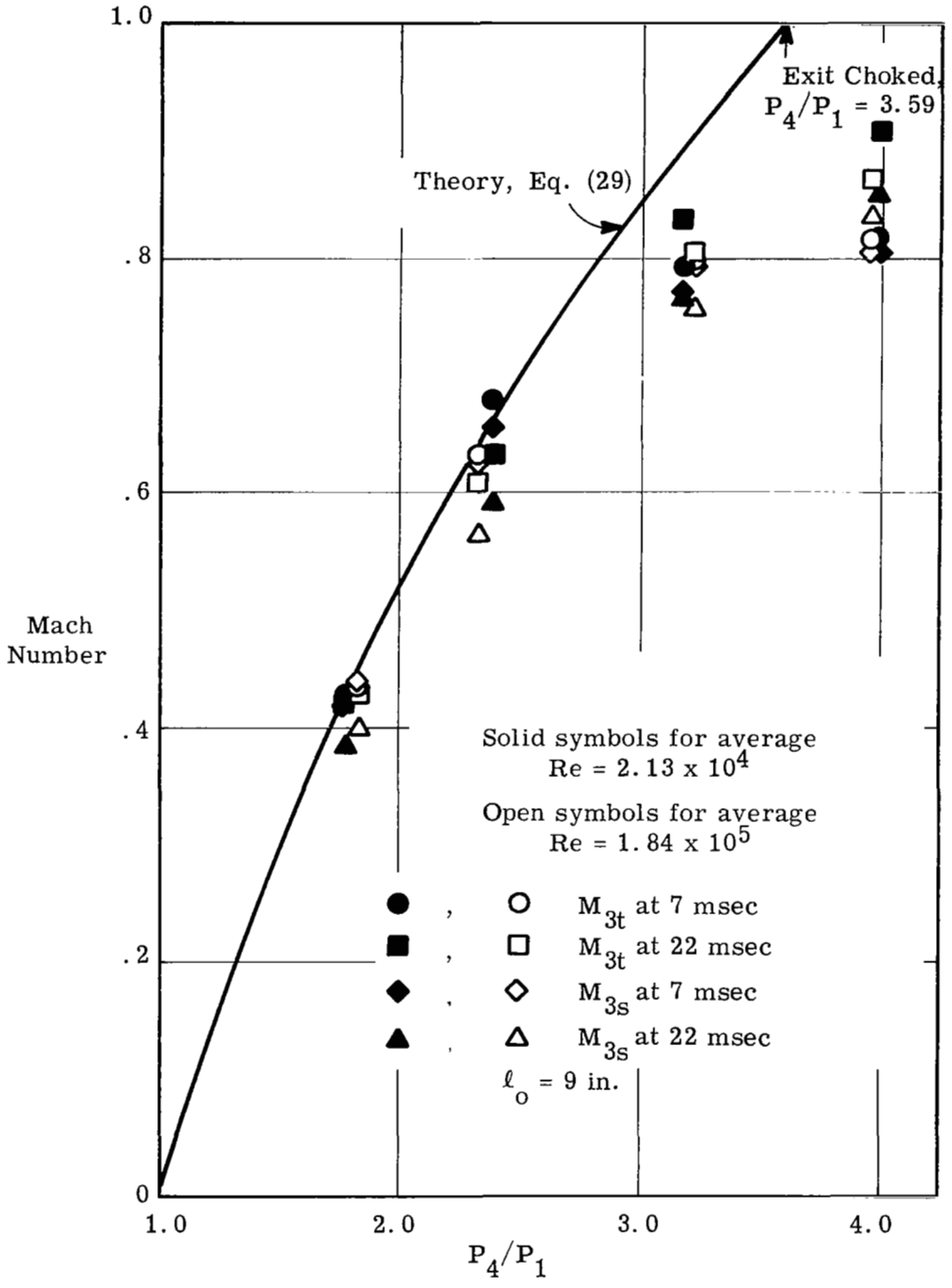

Figure 12. Experimental Flow Mach Number for A_o/A_p = 1.

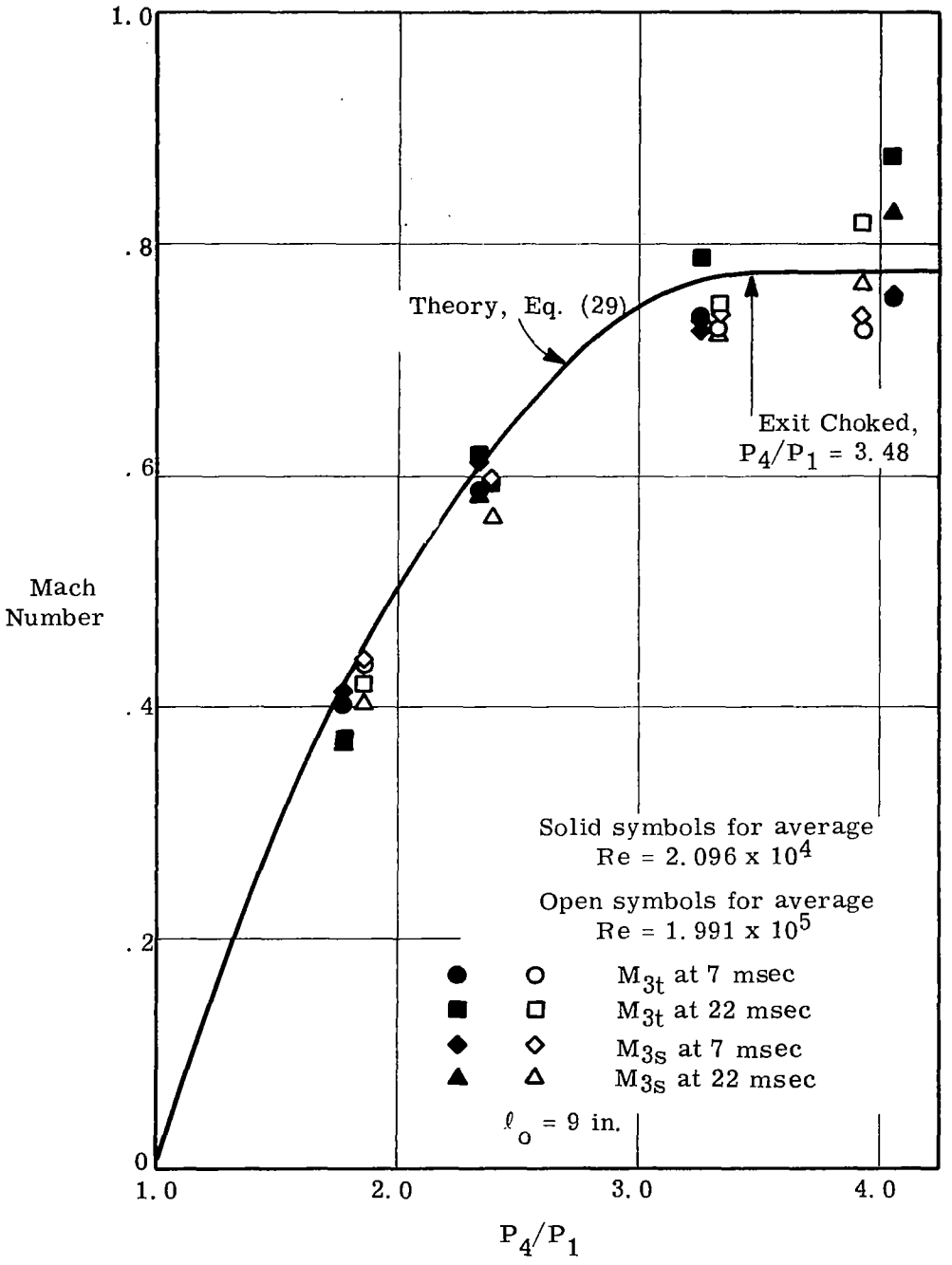

Figure 13. Experimental Flow Mach Number for A_o/A_p = .953

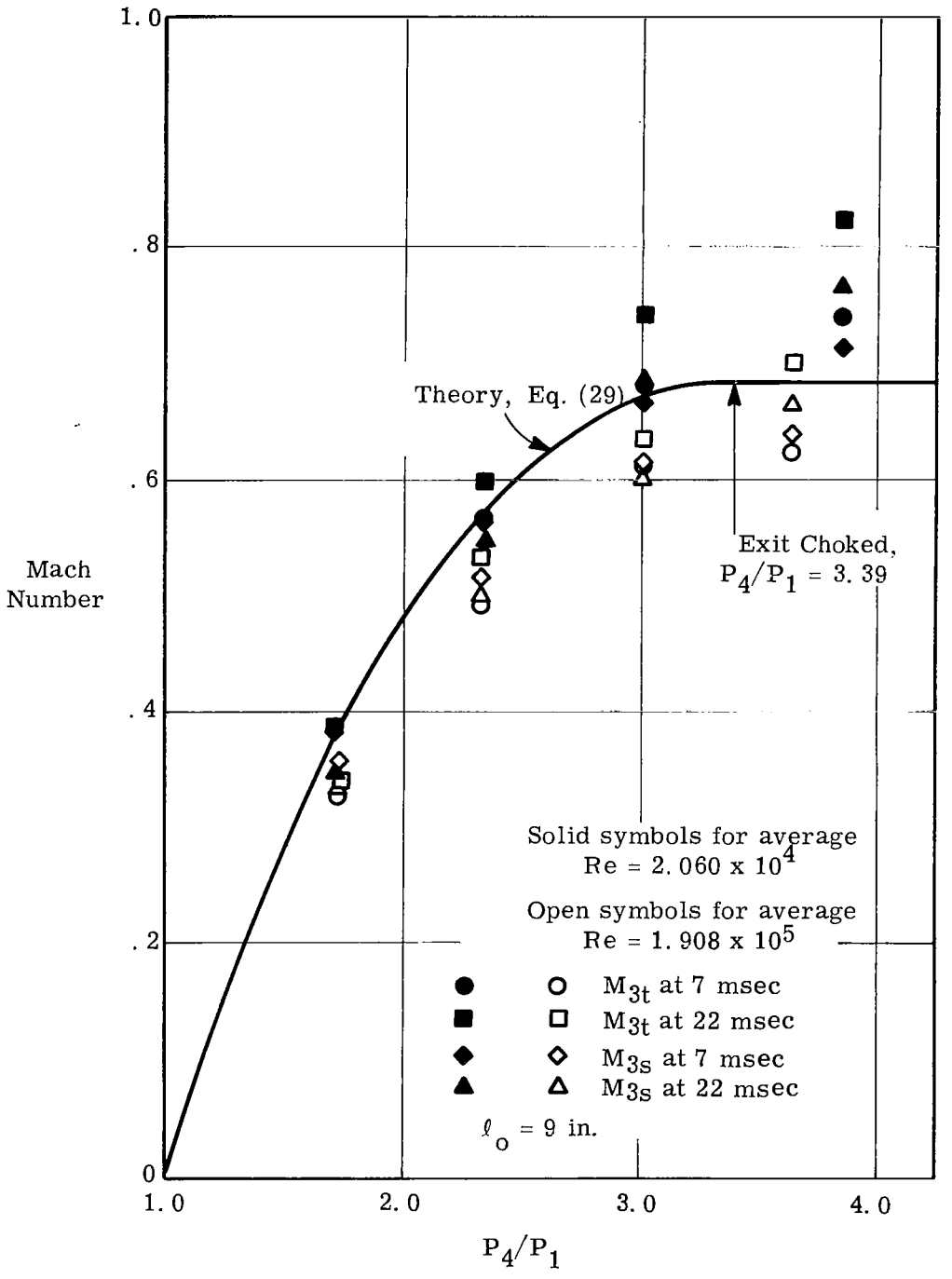

Figure 14. Experimental Flow Mach Number for A_o/A_p = .903

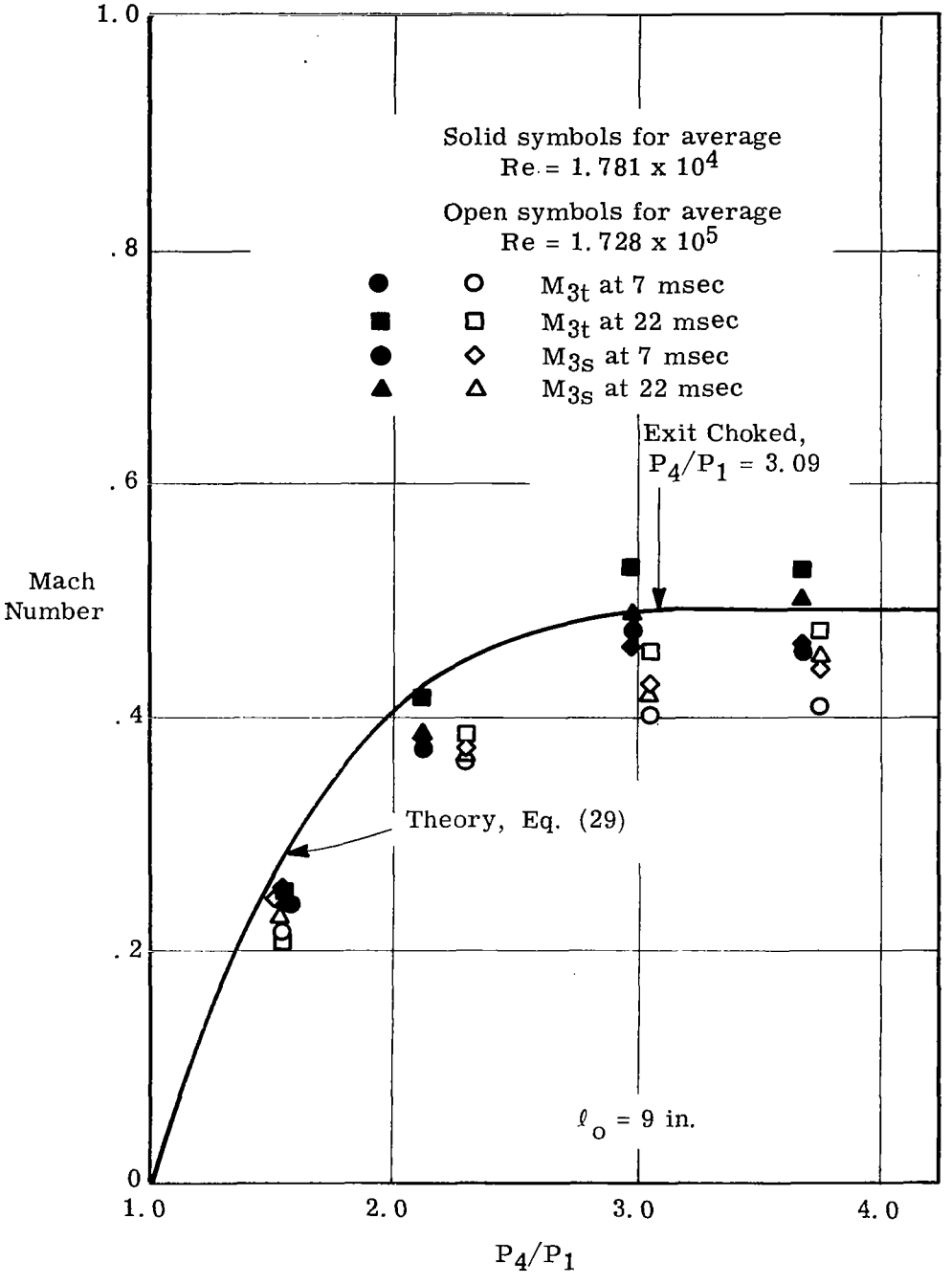

Figure 15. Experimental Flow Mach Number for $A_o/A_p = .737$

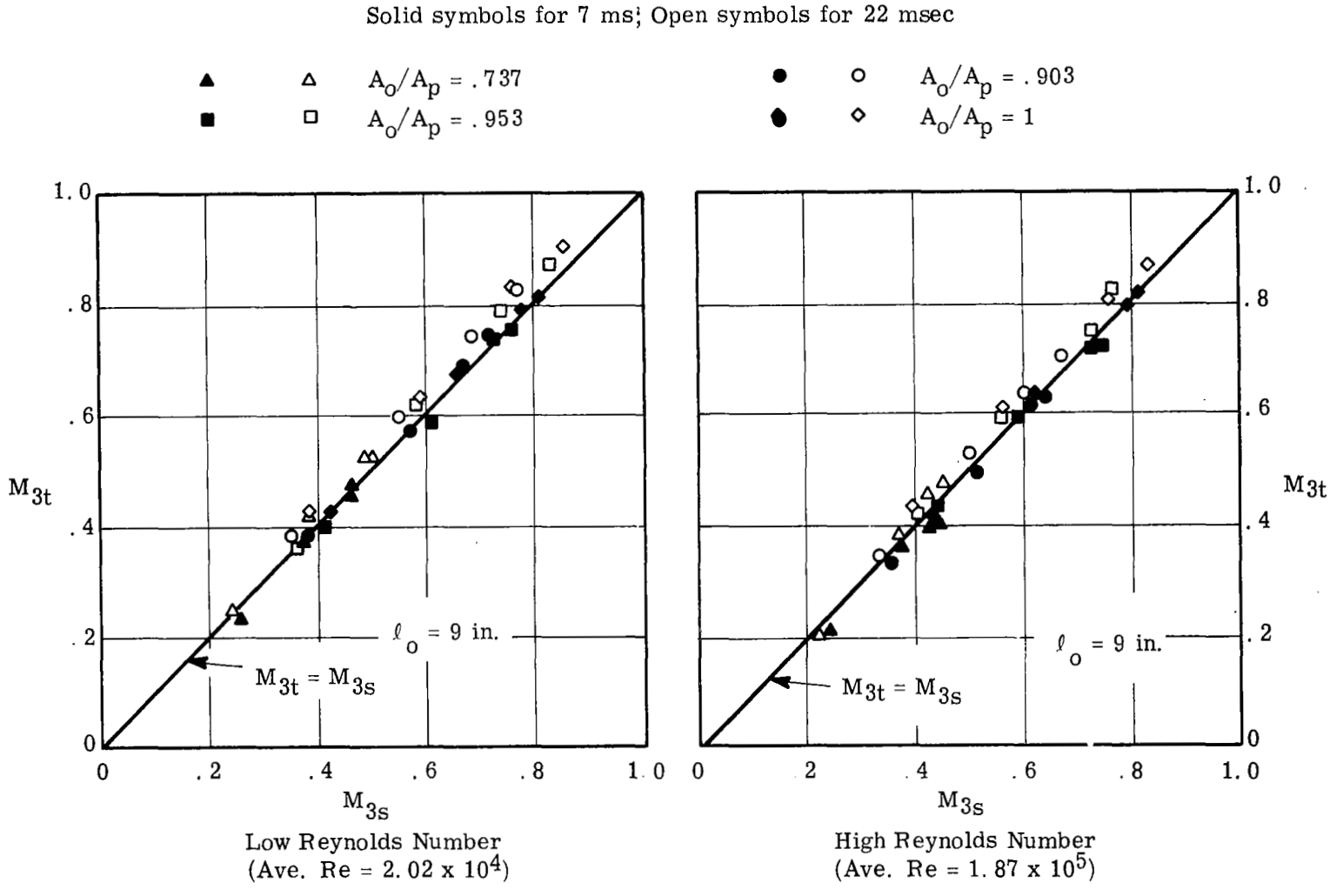

Figure 16. Experimental Flow Mach Number Comparison: M_{3t} vs. M_{3s}

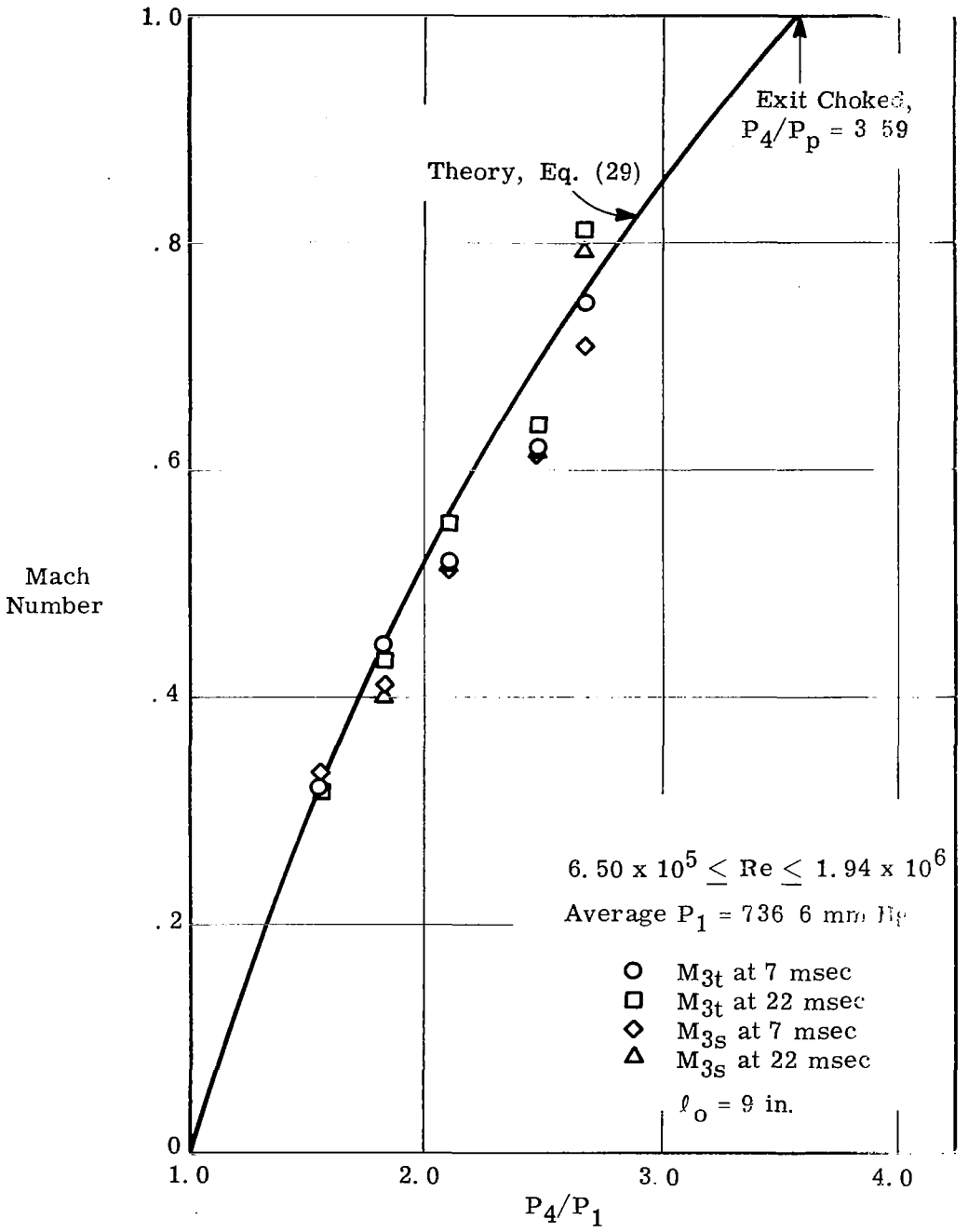

Figure 17. Experimental Flow Mach Number for No Tank and No Orifice

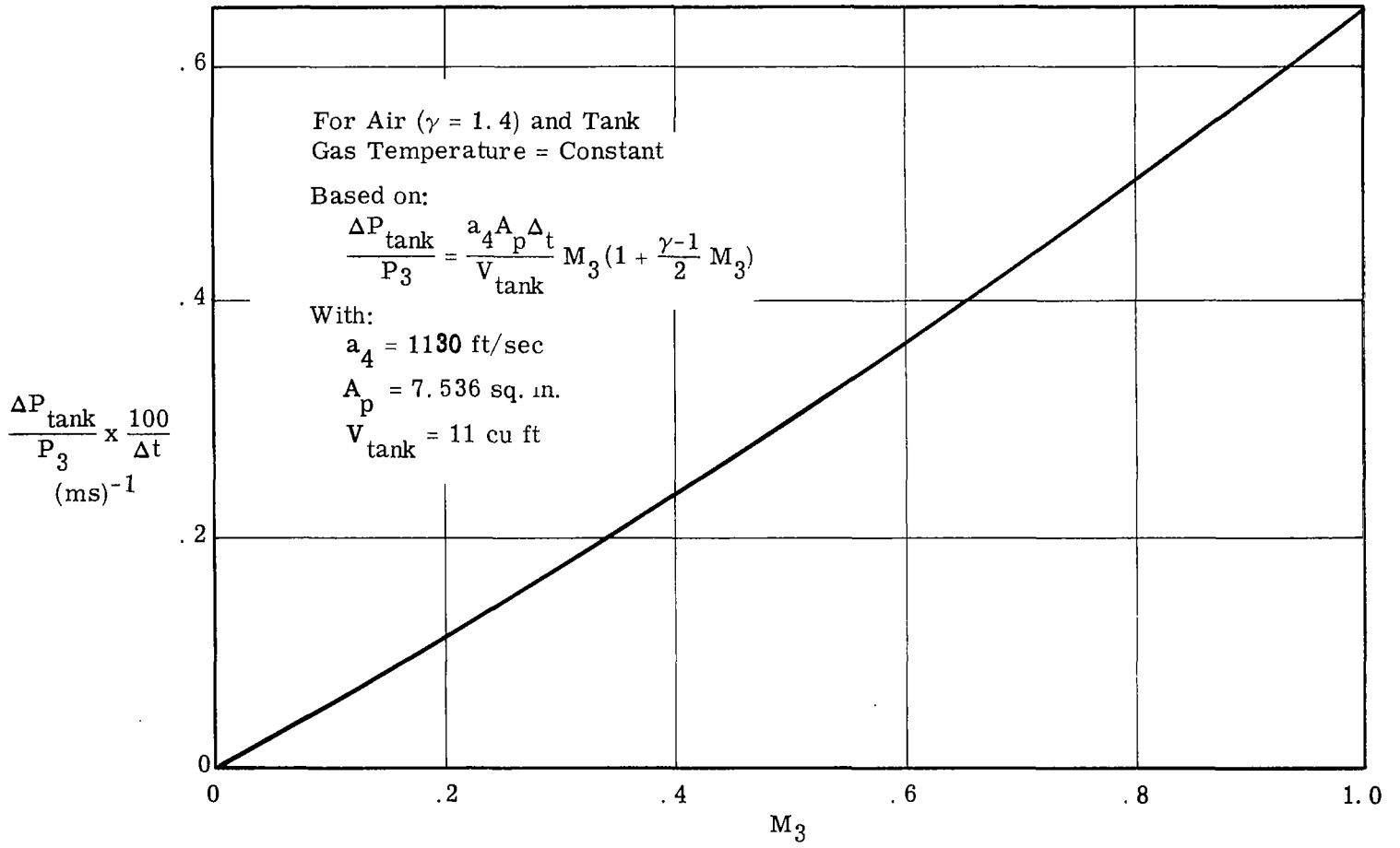

Figure 18. Percentage Increase in Tank Pressure

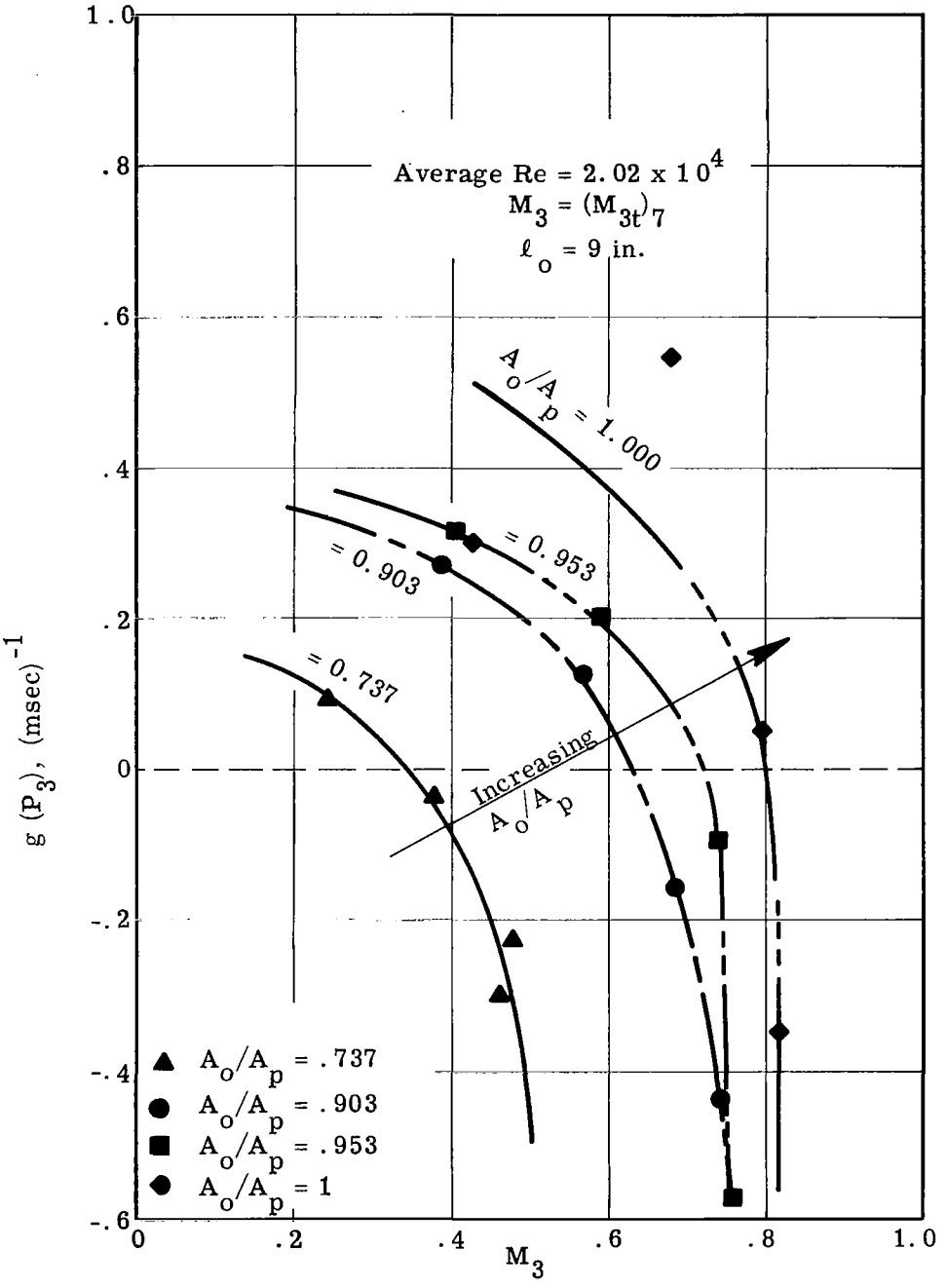

Figure 19. Percentage Change in Pressure—Low Reynolds Number Case

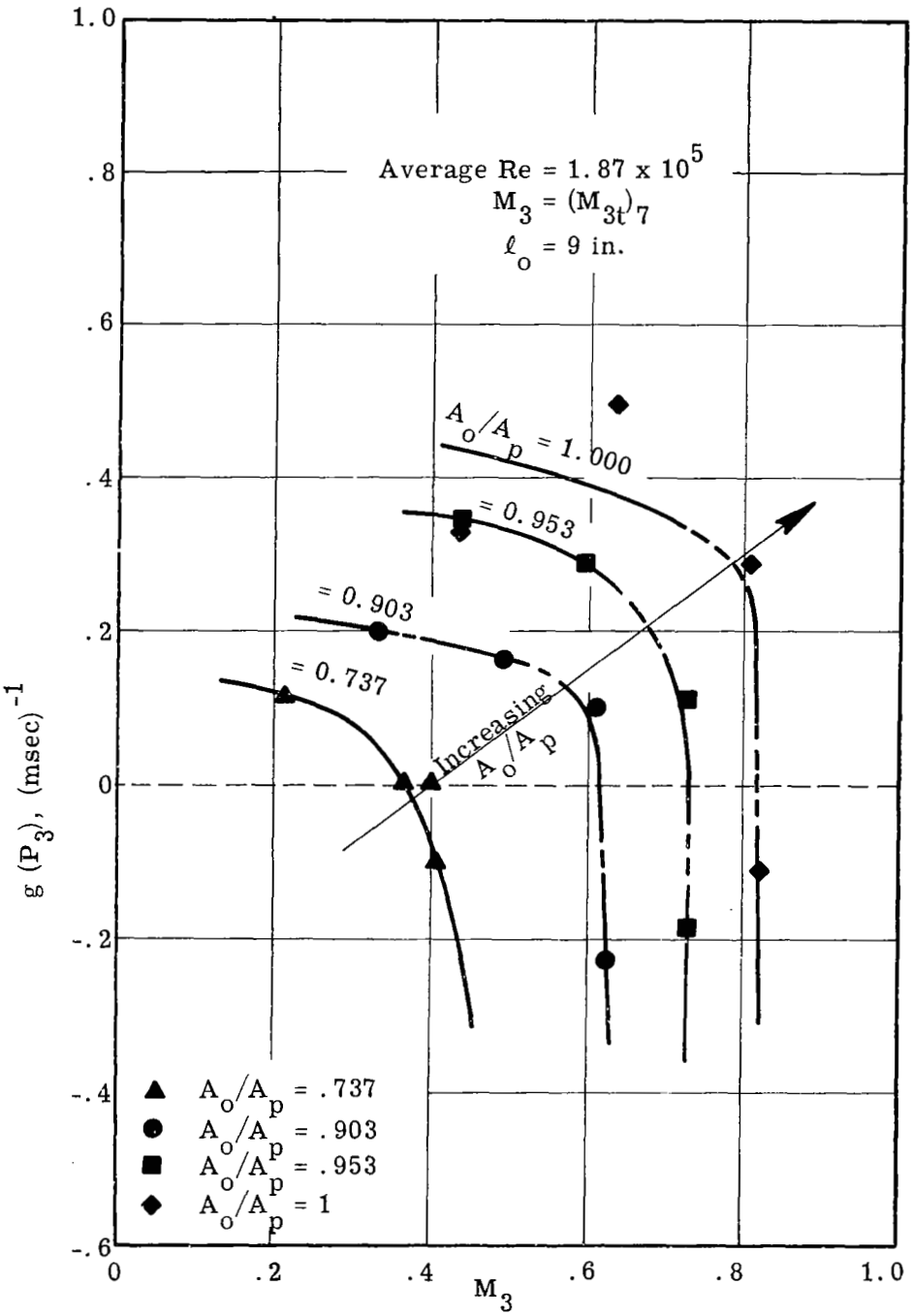

Figure 20. Percentage Change in Pressure—High Reynolds Number Case

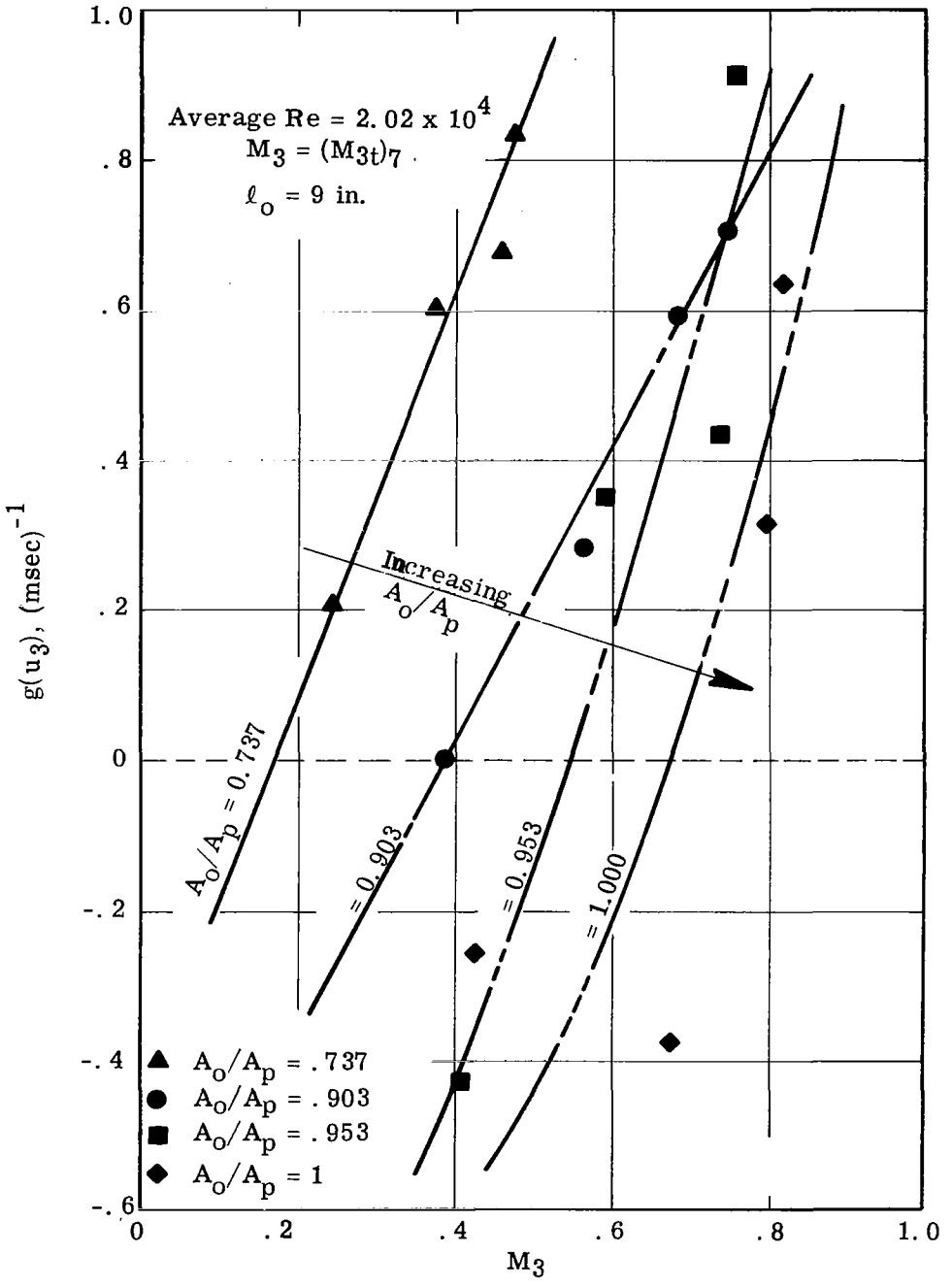

Figure 21. Percentage Change in Velocity — Low Reynolds Number Case

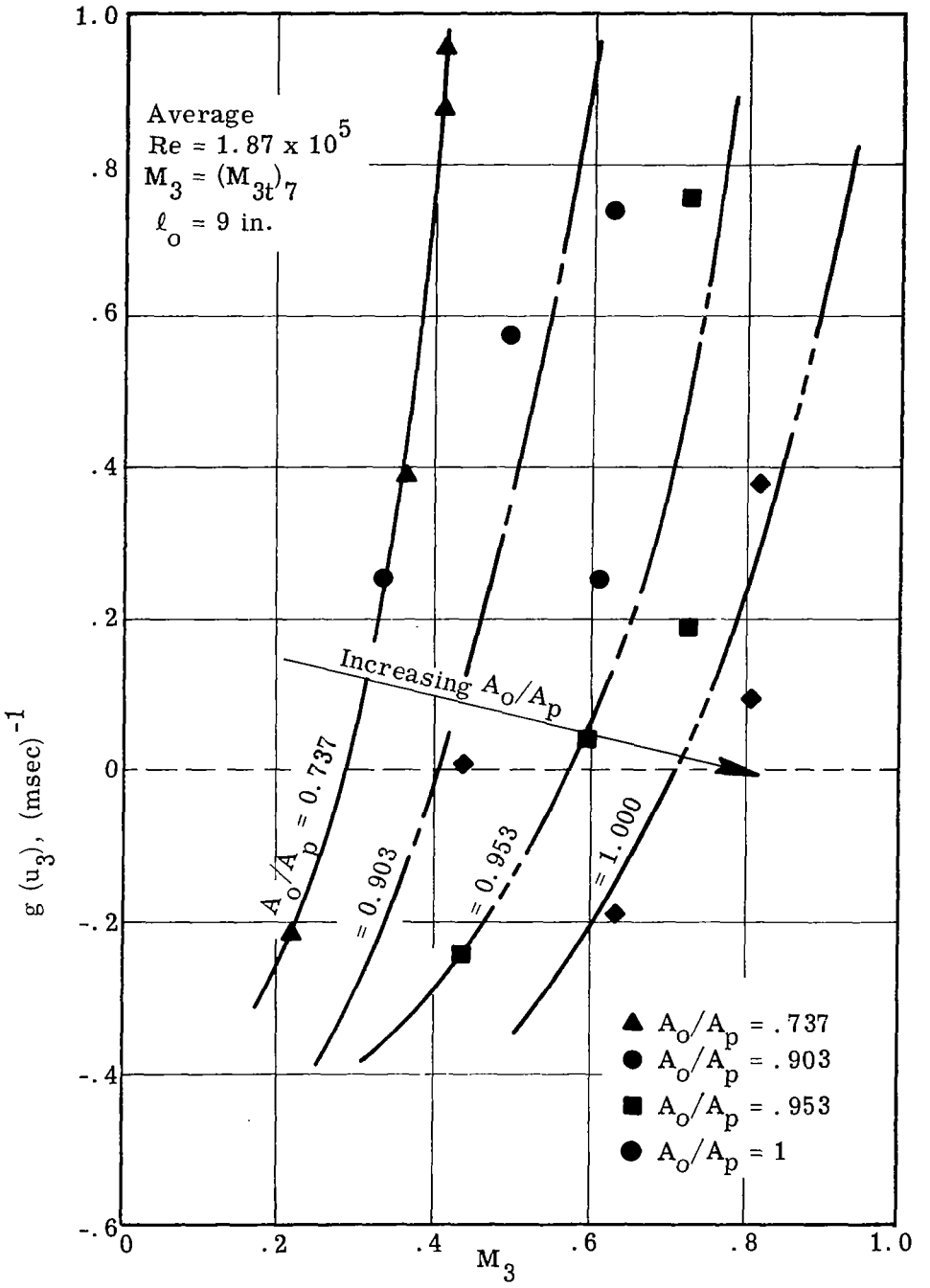

Figure 22. Percentage Change in Velocity—High Reynolds Number Case

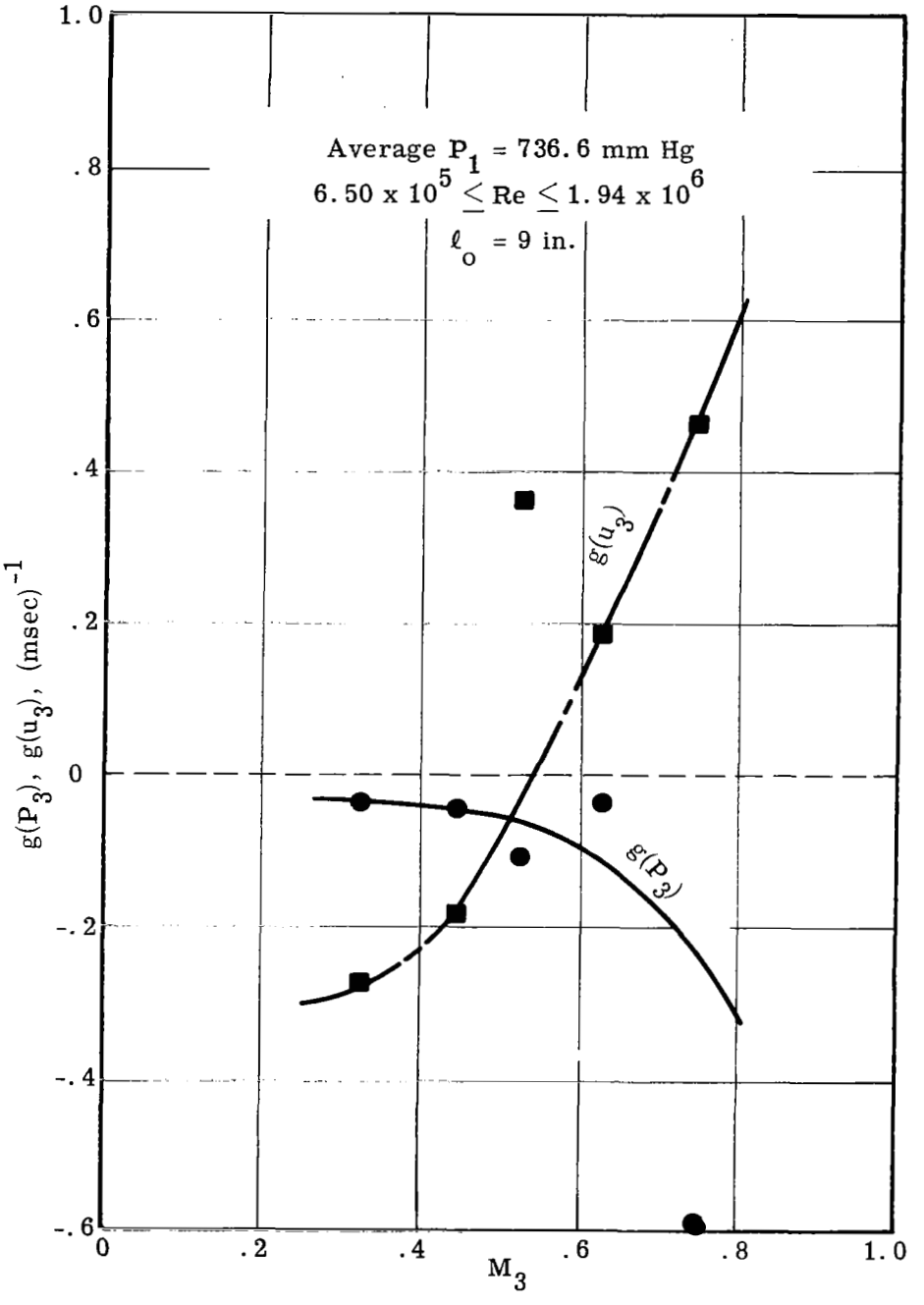

Figure 23. Percentage Change in Pressure and Velocity for No Tank and No Orifice.

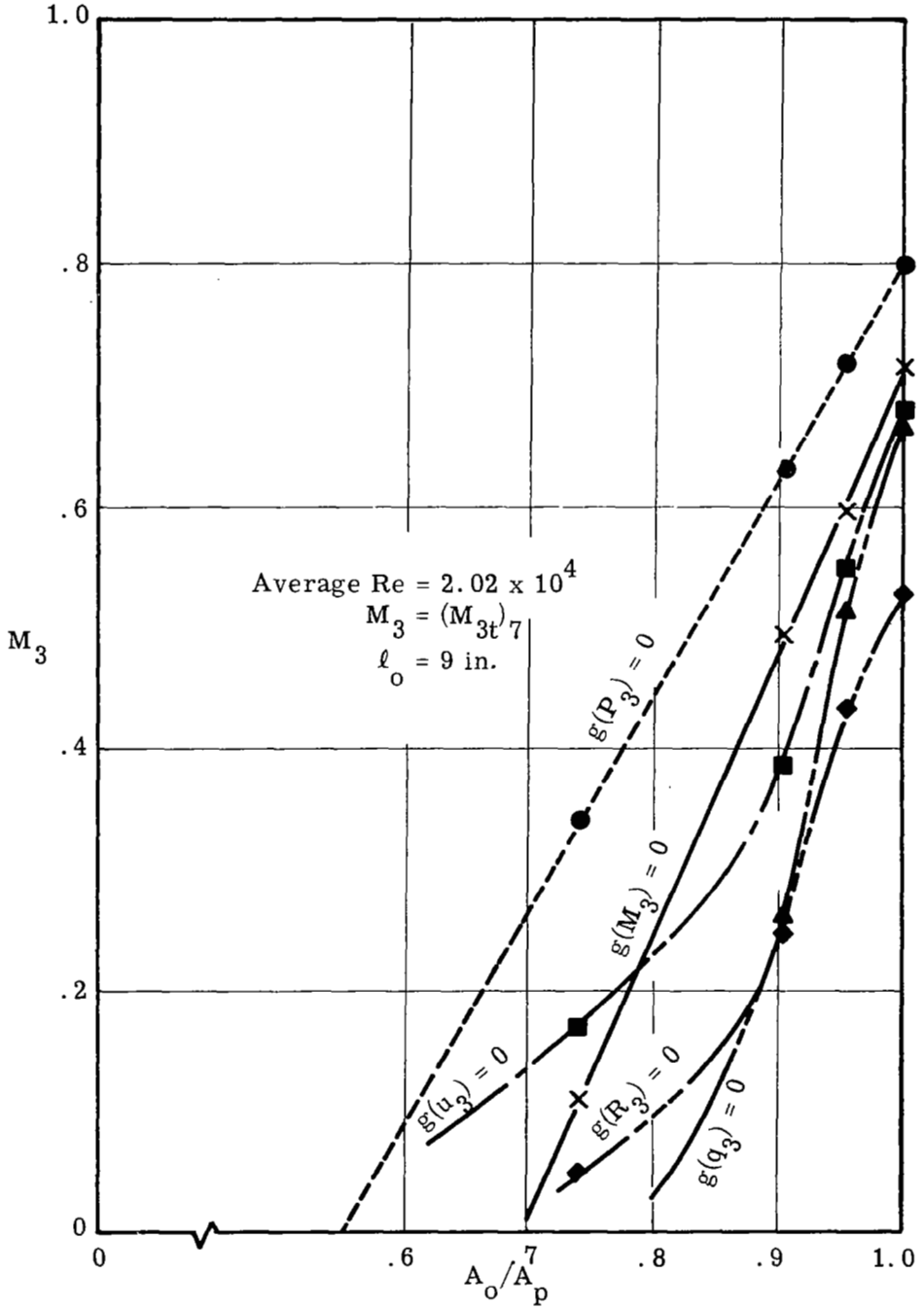

Figure 24. Conditions for Zero Change in Important Flow Variables Behind Expansion Wave—Low Reynolds Number Case

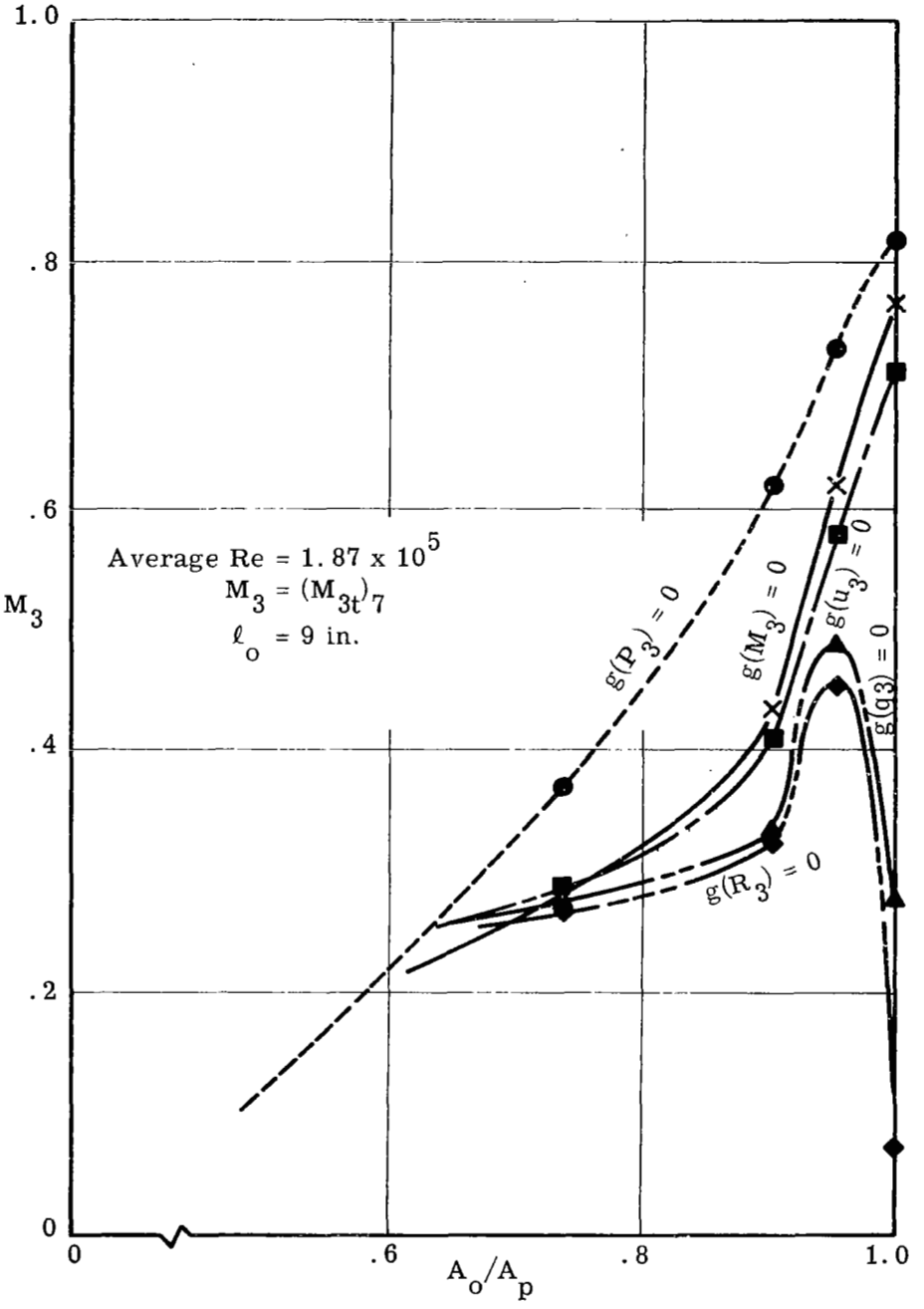

Figure 25. Conditions for Zero Change in Important Flow Variables Behind Expansion Wave—High Reynolds Number Case

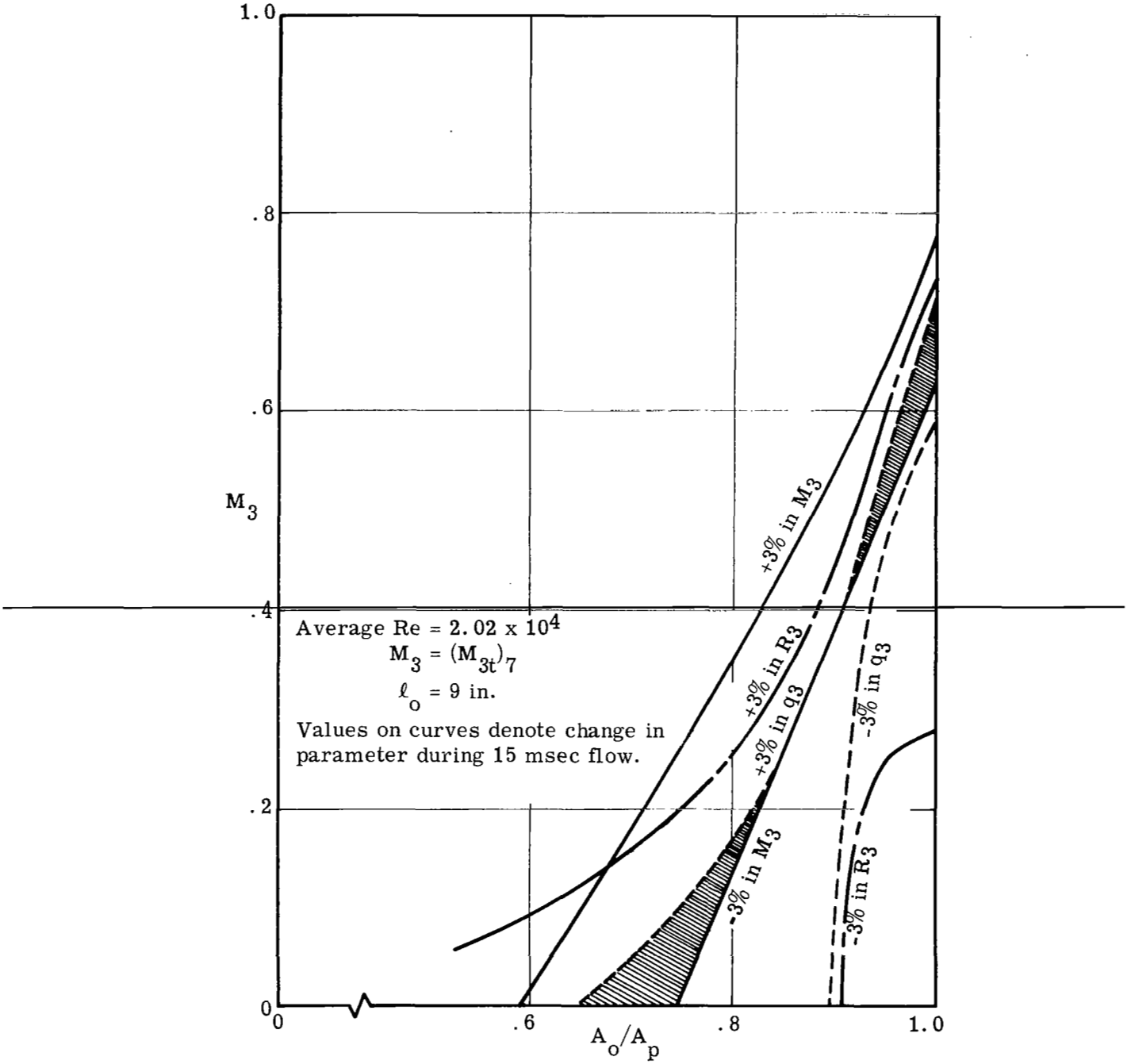

Figure 26. Experimental Operating Range of Expansion Tube for Particle Drag Studies — Low Reynolds Number Case

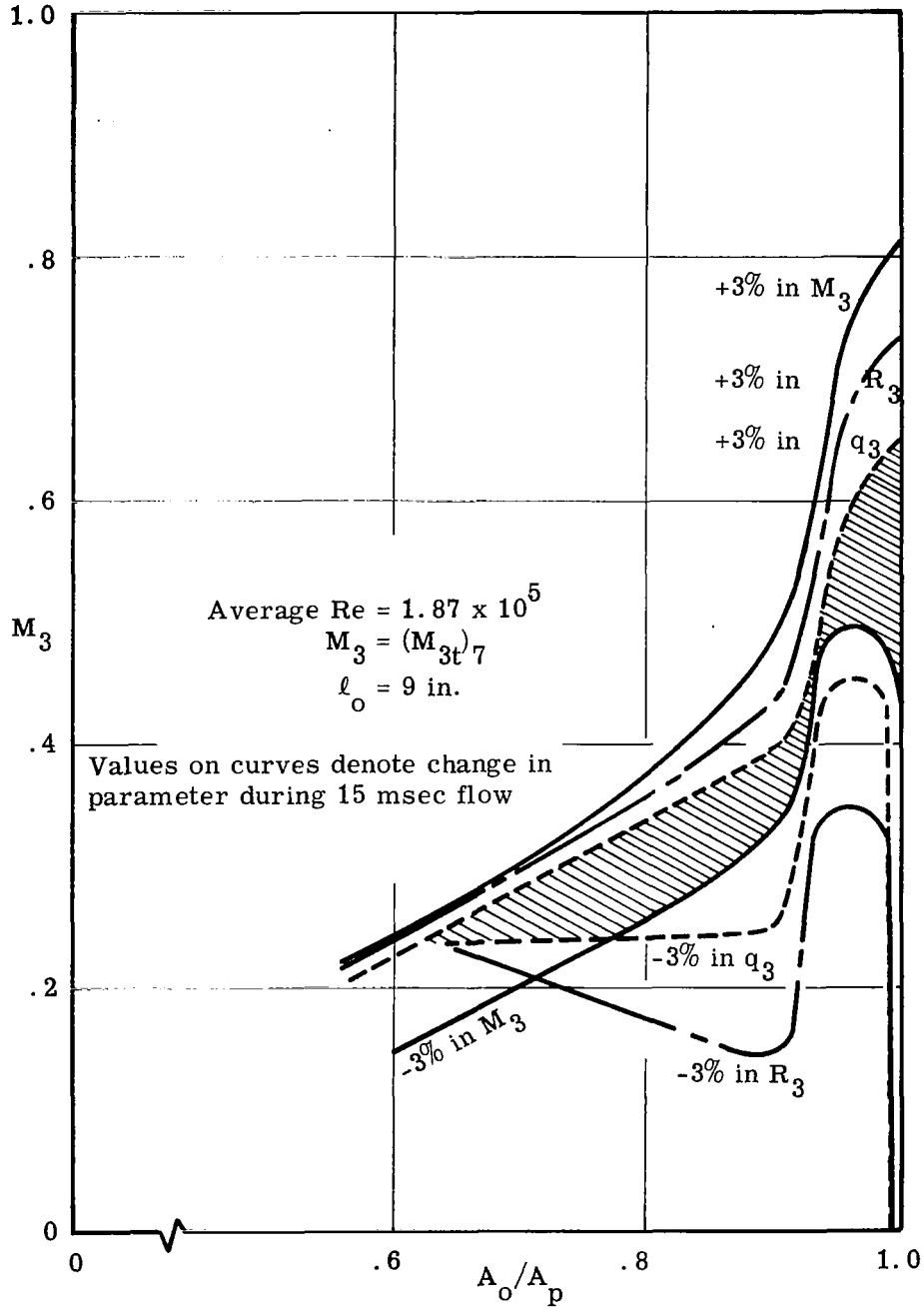

Figure 27. Experimental Operating Range of Expansion Tube for Particle Drag Studies—High Reynolds Number Case

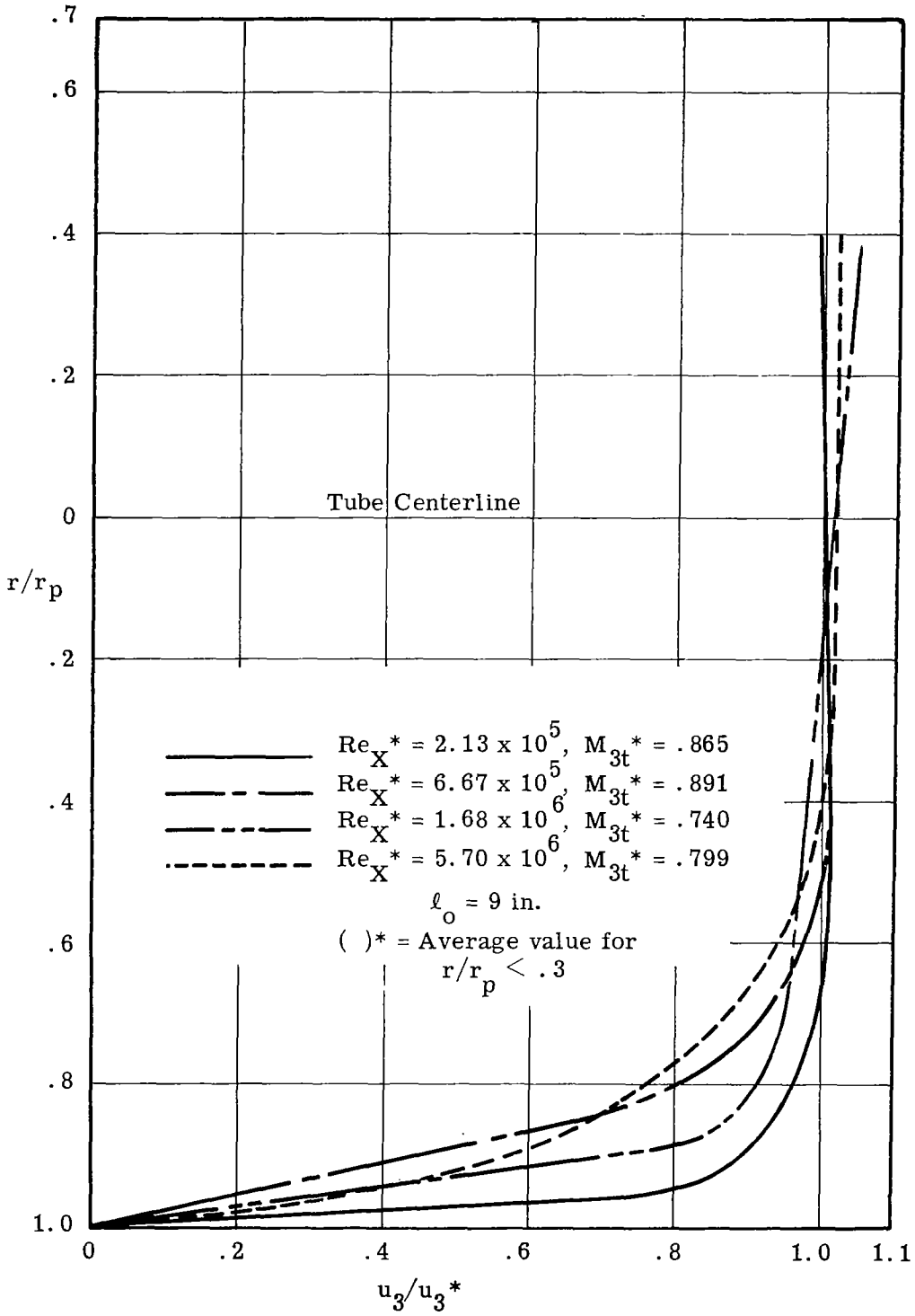

Figure 28. Boundary Layer Profile